Performance Simulation of Vulcanized Natural Rubber based Auxetic Cellular Structures

By

Muhammad Farhan

School of Chemical and Materials Engineering (SCME)

National University of Sciences and Technology (NUST)

2012

Performance Simulation of Vulcanized Natural Rubber based Auxetic Cellular Structures

Name: Muhammad Farhan

Reg. No: 2010-NUST-MS PhD-MS-E-08

This work is submitted as a MS Thesis in partial fulfillment of the requirement for the degree of

MS in Materials and Surface Engineering

Supervisor Name: Dr. Muhammad Shahid

School of Chemical and Materials Engineering (SCME)

National University of Sciences and Technology (NUST)

Islamabad, Pakistan

August, 2012

CERTIFICATE

This is to certify that the work in this thesis has been carried out by **Mr. Muhammad Farhan** and completed under my supervision at School of Chemical and Materials Engineering, National University of Sciences and Technology, H-12, Islamabad, Pakistan.

Supervisor: _____

Dr. Muhammad Shahid

Submitted through,

Principal/Dean,
Materials Engineering Department
National University of Sciences and Technology, Islamabad

To my parents, for everything.

ABSTRACT

Polymeric auxetic foams are formed from conventional polymeric foams when subjected to a compression and heating process which results in the foam re-entrant structure characteristic of auxetic foams. The re-entrant structure imparts enhanced mechanical properties to the material, along with a negative Poisson's ratio, which can be changed by controlling processing parameters. Although the mechanical behavior of these materials is counter-intuitive in nature due to the negative Poisson's ratio, its application in important areas like impact resistance, biological applications, homeland security, sports, etc., makes the creative utilization of its unique properties all the more important. The two-step post-foaming auxetication procedure is applicable to thermoplastic foams, whose base material have a definite softening temperature. However, for thermoset polymers and vulcanized elastomers, a relatively unexplored one step procedure would be required for generation of auxetic cellular structure, in which the auxetic structure would have to be formed prior to final curing of the cellular structure.

The purpose of this research was to develop carbon black nanoparticle reinforced natural rubber vulcanizates, and to investigate the effects of carbon black reinforcement on the mechanical and viscoelastic behavior of the auxetic foam by using modeling and numerical simulation techniques. This has been achieved by mechanically characterizing vulcanized natural rubber of various nanoparticle loadings, and then using the test data to perform finite element simulations on the foam computer generated models. Viscoelastic as well as hyperelastic material models have been used to simulate time-dependent behavior, and large compressive deformation, respectively, by fitting experimental data to theoretical material models in the simulation software. An approximated idealized foam model has been developed based on material properties of the base rubber, and large deformation analysis of this foam structure has been done to determine structural re-organizations, stress distributions, reaction forces, and negative Poisson ratio effect in the foam

structure.

The aim was to characterize the auxetic foams of varying carbon black loading for moderate impact applications. The idealized model developed to study the auxetic structure provides information for further research in rubber based cellular auxetic materials.

ACKNOWLEDGEMENTS

Firstly, I would like the thank the Almighty for giving me the strength, and the means to undertake and complete this research using the best of my abilities.

I offer my most sincere gratitude to my project advisor, Dr. Muhammad Shahid, for this unwavering support, guidance, and encouragement during this research. I would also like to thank Dr. Shamshad Ahmad and Dr. Nasir M. Ahmad for their help and guidance in conducting research in a more efficient manner. The discussions with my class mates and lab technicians have always inspired me to explore different aspects of the research, and for that I am thankful to all of them.

A very special thanks to Mr. Aslam Bhutta, owner of International Polymer Industries Pvt. Ltd., and factory employees for their kindness, and for providing their valuable time and resources to help me with my research.

Finally, I would like to thank my family for their patience, support, and encouragement throughout the course. This work would not have been possible without them.

TABLE OF CONTENTS

LIST OF FIGURES

Chapter 2 LITERATURE REVIEW

LIST OF TABLES

Chapter 2 LITERATURE REVIEW

Chapter 3 EXPERIMENTAL AND SIMULATION SETUP

Chapter 4 RESULTS AND DISCUSSION

CHAPTER 1

INTRODUCTION

1.1 Introduction

Cellular structures exist in nature in various configurations and geometries, and as the microscopic structure of different materials. The factors leading to their formation are different for various materials based on environmental factors, however once the cellular structure in the material is developed, it imparts unique strength, vibration resistance, thermal resistance, acoustic dampening, and various other properties which cannot be achieved by other means. Furthermore, a cellular structure would naturally be lighter than its solid counterpart, and thus would drastically reduce weight for whatever application it is being utilized for. For example, the cellular structure of bone, naturally occurring sponge, coral, the stalk of a plant, all exhibit a distinct open- or closed-cell cellular structure [1].

Synthetic and natural rubber cellular structures have been in use in the industry in the form of impact proof vests, protective and performance enhancing sports materials, vibration damping materials, seat cushioning, and footwear soles. Various variations in rubber compounding, reinforcement, curing and expansion behavior has led to different kinds of materials suitable for various applications. Rubber foam preparation requires complex chemical reactions which have to be correctly timed and controlled in order to get the required properties.

1.2 Auxetic Foams – Synthesis and Application

The development of auxetic foam structure in polymers has largely been focused on thermoplastic foams, and good amount of research has been done in the development of PU based foams. Bezazi and Scarpa have investigated the mechanical behavior of conventional and auxetic polyurethane foams in detail, including studies for compressive cyclic loading [2]. Their investigation includes comparison of the stress-strain behavior of conventional and auxetic foams, their stiffness degradation behavior with cyclic loading, and energy dissipation due to the cyclic loading. Their research develops a good comparison between conventional and auxetic foams mechanical behavior. Chan and Evans also synthesized polyurethane auxetic foams using the compression and heating methodology [3]. They have investigated the effects of synthesis methodology on the mechanical behavior of auxetic foams, and explored the possibility of synthesizing large blocks of auxetic foams, something which would eventually be required for production. Another study by Chan and Evans is an in-depth study about the foam microstructure [4]. They have extended their study of fabrication of the foams by including cell structure analysis, in-situ deformation behavior under an optical microscope, and estimation of cellular mechanical properties through their investigation. Bianchi et al. studied auxetic foam synthesis of a large variety of samples synthesized by varying compression, temperature and cooling conditions [5]. They used the aluminum tube compression method to develop various polyurethane auxetic foam samples. Time-temperature profiles were investigated by Chan and Evans [3], and by Bianchi et al. [5] with the former studying time-temperature profiles and methods of determination, whereas the later focused on optimization of the profiles to determine the ideal auxetic foam formation environment and parameters.

There is, however, a key difference between the way auxetic foams are made from thermoplastic and thermoset materials [6], where the latter requiring an auxetic conversion compression when the foam material is still in the viscoplastic state, which would be immediately prior to vulcanization and post-foaming stage in rubbers. Vulcanized rubbers cannot be converted to auxetic foams by heating and compressing at the base materials softening point, so the conversion needs to take place when the foaming is complete but final curing has just started.

Critical for auxetic foam synthesis would be the microstructure of the pre-vulcanization foam formed, as a foam with too low a foam relative density would give a highly distorted and weak auxetic foam, whereas too high a foam density would make it difficult to convert it into a negative Poisson's ratio material. The proper concentration of the carbon black filler, as will be used in this research, will greatly affect the formation of the initial non-auxetic foam prior to vulcanization, especially when the filler falls in the nanometer range. High surface area of these carbon nanoparticles will increase strength, at the cost of other properties. Proper nanoparticle dispersion during rubber compounding will be critical, as it would affect the way foam cells develop in the final foam. Lakes et al. also synthesized auxetic foams from conventional elastomeric silicone foam, and performed standard mechanical tests to determine Poisson's ratio and foam behavior [7].

Other than cellular materials, auxetic materials have also been recently researched in fibre composite materials using carbon fibre and a polymer matrix for multiple engineering applications [8]. Composite laminated windows have been investigated using ANSYS simulation technology for thin layers of auxetic film sandwiched between other films and adhesives [9]. Composite structures have also been studied by micromechanical simulations with re-entrant and roll-up structures of the inclusions in the matrix material [10]. Open celled cellular structures have also been recently studied for their applicability as sealants in various automotive, defense, and industrial applications [11]. Auxetics, however, do not always favor a particular application, as in the case of the simulation based research done by Whitty et. al. in which they investigated the stresses in thick walled cylinders with different Poisson's ratio, concluding that negative Poisson's ratio materials act as stress concentrators in this scenario [12]. Various research has focused on the mathematical and geometric aspects of auxetic cellular structures in order to understand them from a mechanics viewpoint [13–15], and also to study elastoplastic response using a roll-up auxetic model to study material response in the plastic region [16].

1.2.1 Applications

Elastomeric cellular structures are being used in a variety of applications for vibration dampening, shock absorbency, biomechanics (seating and sports mats), product packaging, and sports shoes, thermal and acoustic insulation, weight

reduction, buoyancy, to name a few [17, 18]. The non-linear elasticity and viscoelastic properties of the base rubber, coupled with the viscoelastic properties of the foam and its lighter weight impart superior mechanical properties for demanding applications. Tailoring foam microstructure by varying blowing agent loading, filler loading, temperature and vulcanization control can help alter these mechanical properties to develop the required foam for the application.

The natural behavior of auxetic materials gives them the ability to restrain, and resist in an counter-intuitive manner, and with time and more research more innovative applications would be discovered for such materials. Fiber pull-out in composites is a common problem, and extensive research is being done in improving adhesion between filler and the matrix, by functionalizing the filler nanotubes, by altering the shape and size of the filler, etc. The natural ability of the auxetic filler would cause it to expand and press against the matrix, during the pull-out phase. This application can help produce rubber auxetic filler polymeric composites which can provide increased strength, fracture, and impact resistance.

Elastomeric materials are known for their vibration and acoustic dampening, and impact resistance. Auxetic elastomeric foams can provide increased impact resistance by absorbing the impact energy instead of transferring it. This property can prove useful in high and medium impact conditions like sports mats and sports shoes, where the human body needs to be protected from damaging impact scenarios. Detailed investigations have been done for such applications using conventional foams which include complex numerical analysis studies [17], and these studies need to be extended to auxetic polymeric materials to verify their suitability as an improvement from their predecessor materials.

1.2.2 Material Modeling and Numerical Simulation

Numerical analysis studies have been performed extensively on elastomeric materials, and an extensive list of material models suitable for most elastomers have been developed, which are used in many commercial finite element analysis codes. Due to the complex non-linear elastic and viscoelastic behavior of elastomers, extensive experimental tests need to be performed to fully characterize mechanical performance for suitability for a particular application. This also requires increased

computation and processing speed, thus pushing researchers to explore more and more innovative and cost-effective ways to simulate the behavior of elastomers. Material models for elastomeric materials and their corresponding foams are usually a combination of hyperelastic and viscoelastic characteristics, and several model parameters are determined which are correlated with the experimental data for a suitable fit. Complicated curve fitting is usually performed by various finite element analysis software, which are widely used in non-linear structural analysis. Elastomeric foams will exhibit fairly complex deformation and stress distribution due to a combination of the non-linear behavior of the base material, as well as the visco-hyperelastic nature of the foam itself, which can be characterized by a combination of a hyperelastic and Maxwell relation model [19]. The fact that auxetic foams have stress-strain curves reported different than conventional foams with the absence of a straight linear region [2] makes them an interesting material for study for the suitability of an existing material model, or the possibility of developing a new one. Homogenized macroscopic properties for the foam can be developed by analyzing the truss like microstructure of the auxetic foams [20], and if sufficient computation power and facilities are available, a three-dimensional scan of the foam can be made using X-Ray tomography apparatus, which can then be used to perform highly accurate finite element analyses on the three dimensional foam microstructure model [21, 22]. Though the later would provide accurate results at the cost of time and computation power, a material model for simpler continuum analyses would be required eventually, since the material would go into production and would be subject to various deformation and stress situations.

Material modeling and behavioral simulation for this new range of materials would provide a better understanding and feasibility of the applicability of auxetic foams to specific situations, and would also pave the way for further computational research.

1.3 Research Motivation

Counter-intuitive materials like auxetic cellular elastomers have enormous potential that is yet to be tapped for utilization in critical impact scenarios, moderate

shock absorbency in sports applications, and as substitutes for conventional rubber foams and rubber materials in mechanical applications. The more the mechanical and complex viscoelastic behavior of these materials is understood, the better it would be for designers to apply it to their applications. Naturally occurring rubber, though being relatively expensive, has a high potential of being used in demanding mechanical applications as it is already widely used in the tire industry, biomechanics industry, and medical applications, and its unique properties have not so far been replicated accurately in synthetic rubbers. Moreover, since it is not derived from petroleum products, it can pave the way for development of biopolymeric auxetic cellular foams that would be used in a variety of mechanical applications. The suitability of cellular auxetic foams as effective viscoelastic dampening materials with counter-intuitive properties has significant potential of being studied under the light of computational mechanics, which can prove to be a useful tool in developing more effective elastomeric material models for these special class of materials. Using finite element analysis techniques at foam microstructure and at a homogenized macro level will not only provide a new arena for computational analysis of materials, it would also help in paving the way for understanding cellular structure formation, structure optimization, auxetic synthesis, viscoelastic and mechanical characterization in light of the new material models developed.

1.4 Objectives

The intent of this research project is to mechanically characterize, and simulate the behavior of a natural rubber based auxetic foam model under different loading conditions using finite element analysis software. A comparison between auxetic foams with varying carbon black filler content will be investigated by using idealized cellular structure models designed in computer aided design software. Base material mechanical properties would be obtained from mechanical tests, the data from which would be used as input for finite element analysis software for material modeling using the products curve fitting tools. The material models developed would be used to investigate the structural deformations, stress distributions, reaction forces, and negative Poisson's ratio effect for the idealized auxetic models developed earlier. This

would provide useful information on the behavior of auxetic cellular structures with varying carbon black loading under different static and time dependent loading conditions.

1.5 Outline

The first few sections of this document are devoted to literature survey related to cellular materials, their synthesis, mechanical properties, and methods by which auxetic foams have been developed in previous research. Later on, mathematical material modeling will be studied briefly, and different material models will be looked into for their suitability for analyzing elastomeric materials. Finally, conclusions derived from this research will be presented in the last chapter followed by recommendations for future work.

CHAPTER 2

LITERATURE REVIEW

2.1 Theory of Cellular Structures

Polymeric materials possess unique properties not present in other materials, due to which their applicability in various structural loading, thermal, electrical and optical applications is highly diverse. Moreover, having relatively simpler processing technology compared to metallic materials gives them an additional advantage in terms of cost reduction for raw materials, and for the equipment employed. Their mechanical and rheological properties have been studied in great detail, and their introduction to general consumer level or sensitive homeland security related applications has prompted researchers to delve deeper into their highly non-linear mechanical behavior, their complex viscoelastic behavior, their integration with a variety of other polymeric materials and their respective configurations to develop even more sophisticated composites and nanocomposites. Recent research has questioned the use of conventional foams for high impact scenarios [23], and also the stress softening effects for polymeric foams due to repeated loading [24], however more sophisticated cellular structures with negative Poisson ratios are expected to give favorable results.

Infusion of regularly dispersed macroscopic or microscopic voids into the bulk of the polymeric material by physical or chemical means will result in a cellular structure. Depending on various processing conditions like temperature, filler loading, forming pressure, the orientation of the “cells” thus formed will result in isotropic or anisotropic material behavior. Generally, for a uni-directional foam rise, the foam would be anisotropic due to the elongation of the foam cells in the direction of the

rise. However, the final foam structure depends entirely on the aforementioned factors, the nature of the base polymeric material, and the processing conditions.

Cellular structures have been investigated by determining foam properties from cellular structures, and various general theories have been laid down, especially in the work done by Gibson and Ashby [1], which allows the estimation of foam behavior by mathematical models. Since polymeric cellular structures are simply the expanded form of the base material, which can be either a form of plastic or a vulcanized rubber, the first and foremost important property clearly visible from the transformation is the significant reduction in density, which has been called the *relative density* for cellular structures. This, and other properties, will be looked into in more detail in the discourse on microstructure examination.

Depending on the processing conditions and the base material, the second important characteristic which identifies the type of cellular structure is the nature of the cells formed. The resulting cellular structure can be either *open-celled* or *closed-cell*. An open-celled foam is relatively less rigid, allows great fluid absorbing capacity, allows gas to traverse through the cellular corridors, and undergoes a very large amount of compression prior to achieving densification. A closed-cell foam, on the other hand, would be relatively more rigid and of greater density due to the presence of cell walls which would enclose the the gas resulting from the decomposition of the foaming agent. Closed-cell structure is also reported to reduce hysteretic loss due to the presence of gas in the foam cells [25]. The reasons for the formation of a closed-cell foam could be less internal pressure of the gases during foaming, relatively lower foaming temperatures, or the presence of a higher amount of filler.

2.1.1 Cellular Configurations

Referring to the text of Gibson and Ashby [1], the various geometrical and mathematical models for the approximation of complex foam structures will be discussed here, since it plays an important role in developing approximate geometric foam models for mechanical properties estimation in this research.

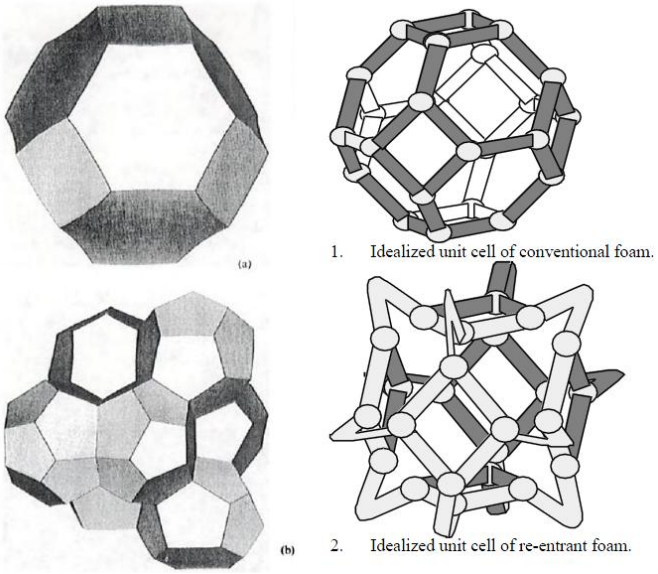

Figure 2.1: Solid tetrakaihedral cell proposed by Kelvin shown in (a), and the least surface area unit cell proposed by Weaire and Phelan (b) [1]. 1 and 2 show the conventional and re-entrant Kelvin cell structures [7].

The general theory underlying foam formation is the minimization of the surface area of the cell. Although Gibson and Ashby have proposed a cubic structure to approximate a foam cell, the actual cell shape is far different from that, and forms complex multi-faceted shapes which have no definite orientation or symmetry. However, by accommodating surface area reduction factors in geometry determination, and considering the processing conditions, one can reach an approximate geometric model. Lord Kelvin [26] proposed the tetradecahedron cell, which is a polyhedron comprison of six square and eight hexagonal faces, all of them curved. Figure 2.1 shows how the cell has been shown in its original form, and then in a modified re-entrant structure, which is basically the same cell with its ribs deformed at the center to give the cell a negative Poisson's ratio. The re-entrant structure will be discussed in more detail later in this text. The Kelvin cells are arranged in a BCC arrangement as per Lord Kelvin's conjecture.

However, later work by Weaire and Phelan showed that a unit cell comprising of a unique arrangement of tetrakaidecahedron and dodecahedron cells has a surface area 0.3% less than the Kelvin model [26]. The unit cell of the Weaire and Phelan model consists of six 14-sided polyhedra and two 12-sided polyhedra, and is currently considered the foam model which requires the least surface area.

Generally, the real foam structure has varying cell sizes, and the size distribution homogeneity as illustrated by these models is not present in physical open or closed-cell foams. Random cell nucleation positions throughout the polymer continuum would result in considerable cell size variations, and would result in a Voronoi spatial tessellation which implies that the cell nucleation was random, but their respective growth rates were linear [1]. These Voronoi type tessellations have recently been investigated by numerical techniques for auxetic and non-auxetic structures, for a material with anisotropic behavior [27]. Cellular morphology and size distribution will depend on how well the fillers were dispersed, as filler loading variations throughout the continuum will result in "hard and soft" areas which would restrict or allow the growth of foam cells, respectively. The focus of this research is on carbon black reinforcement effects on the negative Poisson's ratio cellular structure, and the performance of the final auxetic foam will highly depend on the way carbon black loading played its role in the foaming of the rubber.

2.1.2 Cellular Characterization and Modeling

Foam cellular structures are usually studied under high and low magnification to investigate cell size variation, distribution, cell ribs and wall dimensions, foam rise effects (anisotropy), cell shape, mean cellular dimensions, and relative density. It is imperative that cellular characterization is done thoroughly in order to determine macroscopic mechanical properties with greater accuracy. Foam materials serve to reduce weight, to provide structural and acoustic damping, and in a high level of absorbency, which necessitates the determination of the important property of *relative density*, defined as the ratio of the density of the foam to the density of the solid material the foam is made of. Gibson and Ashby have related the relative density ratio to the ratio of the elastic modulus of the foam to the elastic modulus of the base material as follows:

$$E^*/E_s = C_1 \Phi^2 (\rho^*/\rho_s)^2 + C_1^* (1-\Phi) (\rho^*/\rho_s) \qquad (2.1)$$

Where, E^* = Elastic modulus of the foam

E_s = Elastic modulus of the base material

C_1 = Constant of proportionality

Φ = Fraction of the solid contained in the cell edges

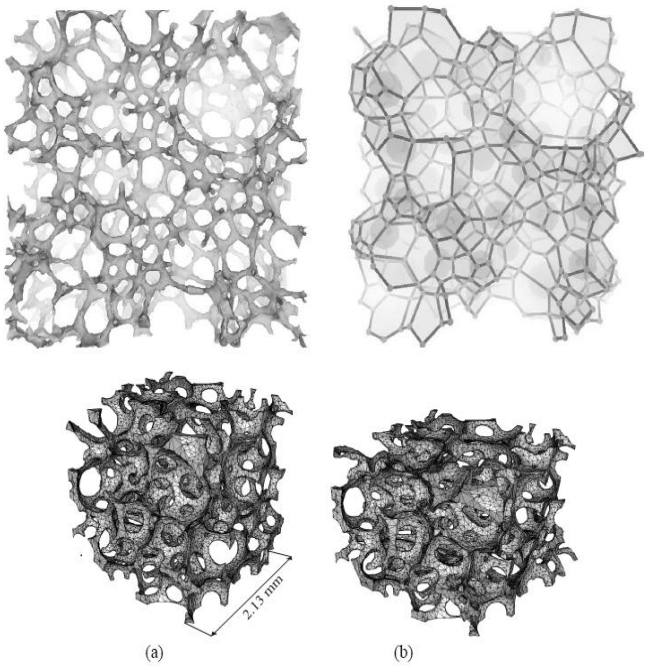

Figure 2.2: Top two images show the foam structure obtained by microtomography and its corresponding stick model [28]. (a) and (b) at the bottom show the actual and compressed 3D foam microstructures also determined using microtomographic techniques [21].

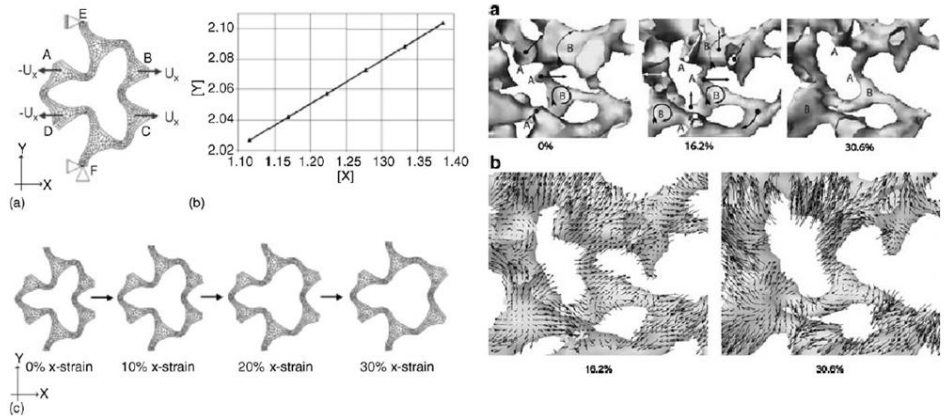

Figure 2.3: The series of images on the right show the work done by Grima et al to verify their theory of rotating joints using FEA [29]. Images on left show actual microtomographically obtained auxetic structure subjected to tensile deformation in work done by McDonald et al, exhibiting the same phenomenon of rigid joint rotation and cell bending [22].

ρ^*/ρ_s = Relative density of the foam

Closed-cell elastic properties determination is more complex than open-celled foams due to the gas pressure enclosed by the cell walls and the mechanical behavior

of the walls themselves (stretching and wrinkling). The above relationship had been developed by Gibon and Ashby based on these considerations. It should be noted that Gibson and Ashby used their cubic cell model to develop this relation. Various other relationships pertaining to non-linear elastic response, densification, and energy absorbency were also developed by the authors, and they will be reviewed in the section on conventional and auxetic foam mechanical properties.

Scanning Electron Microscope (SEM) images are standard two dimensional images, and though the depth of field gives an idea about the three-dimensional structure of the foam, it is still not easily possible to determine an accurate geometrical model of the foamy structure. The process would complicate even more for auxetic foams. Imaging techniques like X-Ray Tomography has been used on polyurethane foams to scan foam microstructure, which is then used in finite element analysis programs to determine foam mechanical behavior. Three-dimensional structures of polydisperse polyurethane open-celled foams were developed by X-Ray Tomography, which helped in generating "stick figure models" of the foams, approximating the skeletal structure, and these were used to determine small structural variations in the foam model [28]. This has been reported to provide essential internal microstructural information, but it is still a process that requires refinement and research, since the development and interpretation of the three-dimensional models is computationally intensive, and X-Ray microstructural examination techniques are yet to be established as a standard for cellular structure examination. Viscoplastic polymeric foam behavior has also been analyzed by deforming two-dimensional "slices" of the foam microstructure, and also using a three-dimensional meshed foam microstructure under compressive loading [21]. The microstructures were scanned using X-Ray Tomography which resulted in the voxel (three-dimensional pixel) based image. The three-dimensional foam compression finite element model provides vital information for foam compression behavior, the buckling of cell ribs during deformation, and the distribution of stresses throughout the cellular structure. Generally, polymeric foam materials have mechanical and viscoelastic property contributions from the base polymer material, and from the structure of the foam. So the mechanical and viscoelastic behavior depends on both the individual properties of the base polymer, and on the behavior of the cell structure.

Bent struts were observed in polyurethane open-celled auxetic foam tensile deformation of their corresponding micro-structural models obtained from microtomography [22]. Particular importance is given to the use of this technique to understand in greater depth the phenomenon of rigid joint rotation and buckling of ribs in auxetic foam deformation, a theory proposed earlier by Grima et al in their research on negative Poisson's ratio polyurethane foams deformation behavior [29]. Though the theory and its verification in the microtomography experiment highlight the deformation phenomenon in auxetic foams, the reason behind this mode of deformation can be understood by the fact that during the foaming process a major portion of the solid polymer is concentrated in the “nodes” of the cells, whereas, due the excessive extension, the walls and ribs get thinner in their central portions, leading to susceptibility to deformation at these portions of the ribs and walls, while the nodes remain largely undeformed.

Auxetic cellular structure development has also been investigated for bulk production for different surface curvatures, which can be used for a variety of applications [30]. For applications related to the automotive industry, non-pneumatic tires have been studied for honeycomb type cellular configurations and with an auxetic structure of the struts that make up the inside of the special tire [31].

The aforementioned research provide an idea about the importance of cellular characterization in understanding the bulk behavior of the cellular material. Other than the relative density of the foam, geometrical parameters like cell shape, edge and face connectivity, face and edge thickness, material in cell edges, largest and smallest principal dimensions, cellular anisotropy, and structural symmetry are required to fully understand the bulk behavior [1]. Prior to developing three-dimensional models of the foam, these cell parameters need to be determined.

2.2 Carbon Black: The Reinforcing Nanoparticle

Composite materials are an essential requirement for modern applications, since they provide the synergistic effect of a group of materials put together to form one composite. Generally there are two components to a polymeric composite material; the matrix, and the filler. The filler serves the purpose of imparting different properties to the polymer by dispersing throughout the matrix continuum. The

dispersion effects the homogeneity of the desired properties in the composite material, and hence material processing conditions like mixing, temperature control, polymer viscosity play an important part in determining how well the reinforcement is dispersed in the matrix. Cellular nucleation in the synthesis of polymeric foams is also affected by uniform dispersion of these nanoparticles, since they act as effective nucleation sites, and their presence in the ribs and walls of the cellular structure would ensure better reinforcement for the otherwise weak microstructure [32]. Dispersion becomes a challenge when the filler dimensions are a few nanometers, since the properties of particles changes at the nano-scale, thus affecting matrix-filler interaction considerably.

Carbon black dispersions in the rubber matrix are in the form of particle aggregates, and not individual carbon black particles themselves, since the high surface energy of these nano-sized particles causes them to adhere to each other. This can, of course, be a cause of concern if the particle size is too small, thus decreasing material properties homogeneity. Essential parameters like surface area, surface structure, size distribution of aggregates are determined by very high microscopy techniques like TEM, and by various standardized chemical adsorption methods, like nitrogen, cetyl triethyl ammonium bromide, and iodine adsorption for determining the surface area, and TEM, dibutyl phtlalate adsorption, and mercury porosimetry for structural characterization [33]. Recent research has also delved into the combined effect of other nanoparticles like nanobarite have led to enhancement of final products properties [34], and cure rate index of NR-filled compounds was improved by using waste gypsum obtained from waste plaster molds [35].

Carbon black particle morphology is compared to that of an onion like structure of graphitic layers overlapping each other to form the particle, with the graphitic order decreasing towards the center of the particle, as shown in Figure 2.4 [36]. This has also been shown by STM imaging, as shown in Figure 2.5 [33]. The serrated edges signify unsatisfied carbon bonds which lead to tendency for chemical reactivity. Individual dispersion of carbon black particles or smaller agglomerates are classified as *low structure* carbon black, whereas larger agglomerates with a certain degree of branching of the agglomerated chains. As stated earlier, this structure is of importance in the behavior of carbon black in the polymer matrix.

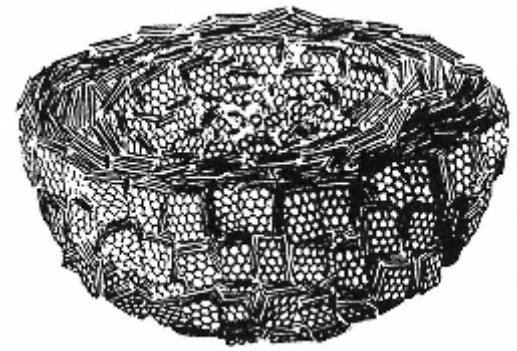

Figure 2.4: The cross-section of a carbon black nanoparticle showing the decreasing order of graphitic layers towards the center [33]

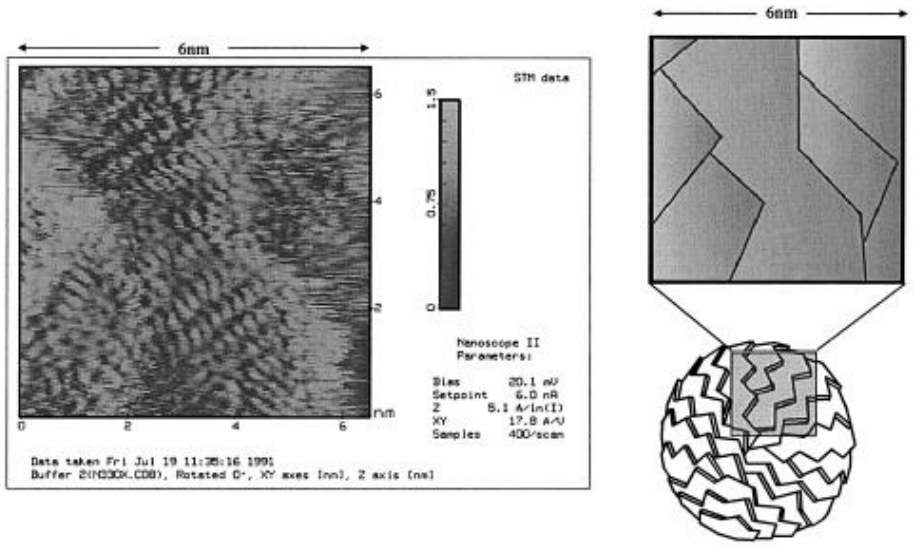

Figure 2.5: Carbon black surface imaging using STM. The image shows the onion like structure of the particle made by the graphitic layers [33].

ASTM numbers	Primary particle diameter (nm)	Previous nomenclature
900–999	201–500	MT: Medium Thermal
800–899	101–200	FT: Fine Thermal
700–799	61–100	SRF: Semi-Reinforcing Furnace
600–699	49–60	GPF: General Purpose Furnace
500–599	40–48	FEF: Fine Extrusion Furnace
400–499	31–39	FF: Fine Furnace
300–399	26–30	HAF: High Abrasive Furnace
200–299	20–25	ISAF: Intermediate Super Abrasive Furnace
100–199	11–19	SAF: Super Abrasive Furnace
000–099	1–10	—

Table 2.1: Carbon black nomenclature based on ASTM standards [36]

The type of carbon black synthesized depends largely upon the manufacturing process used. For example, the carbon black used for the manufacture of tires is done by the thermal process which yields large low structure particles. Applications requiring a high degree of improvement in toughness and modulus would require finer particles with a better agglomerate structure. Based on the manufacturing process employed, different grades of carbon blacks are yielded, and carbon black nomenclature based on ASTM standards is tabulated in Table 2.1.

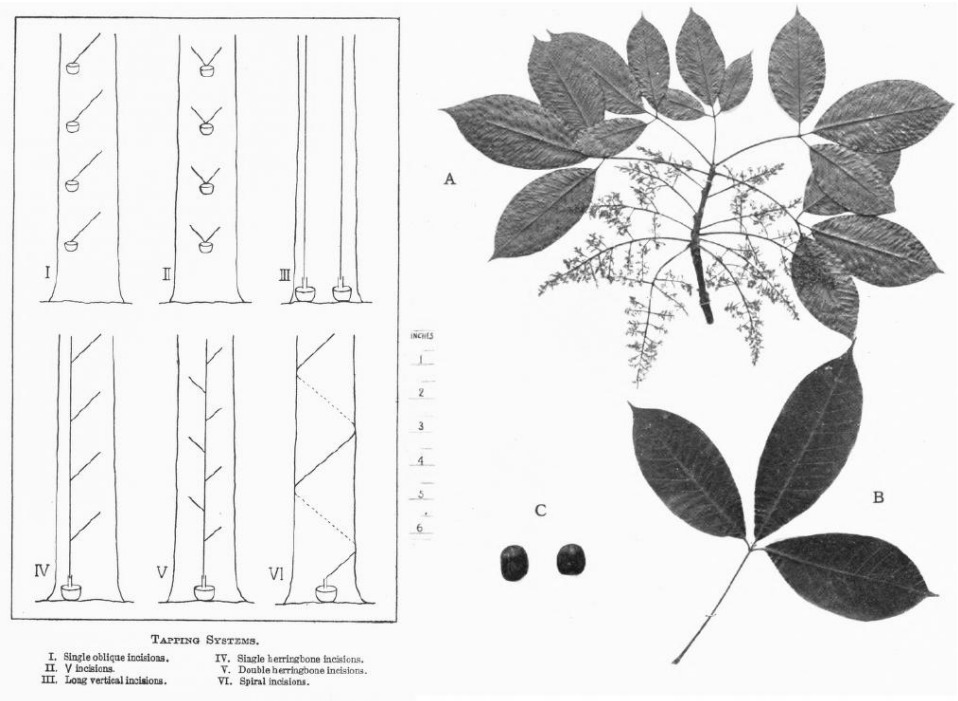

Figure 2.6: Methods of para rubber (Hevea Brasiliensis) tree incisions, and the leaves of the tree itself [38]

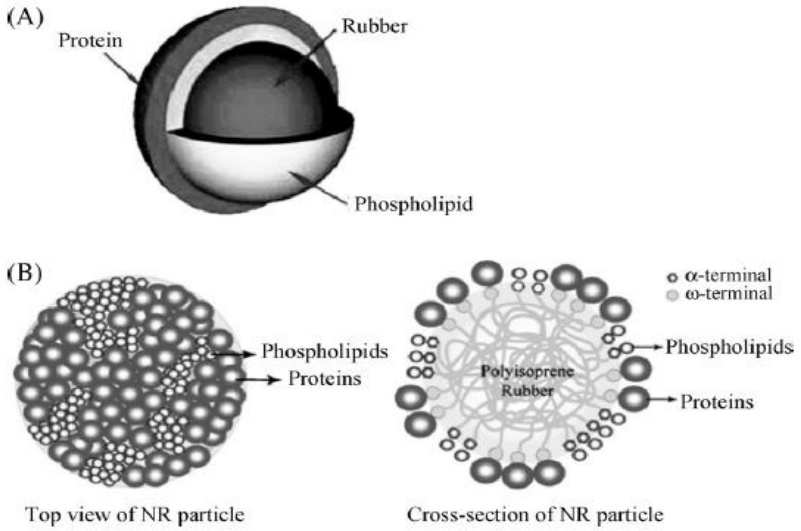

Figure 2.7: Two possible structures of the latex NR particle surface. The mixed layer model was verified by Nawamawat et al by surface characterization techniques [41]

2.3 Natural Rubber

Being a bio-polymer, natural rubber is initially derived in viscous liquid form from particular rubber trees. This fluid is generally referred to as *Latex*, and it has to be pre-processed by filtering, drying and baking operations to be rendered of any use as a rubber. Latex is basically a watery emulsion containing globules of the rubbery substance, and is said to possess a bimodal molecular weight distribution, and it is dependent on the very initial processing conditions [37]. It is extracted from the tree *Hevea Brasiliensis*, popularly known as the *para rubber tree*. Countries exporting natural rubber bales are Malaysia, Indonesia, India, among others. Due to the extensive application of the rubber in the tire industry the rubber bales obtained from these countries are forever in demand, and a decreasing supply of natural rubber to the world rubber industry could stem from multiple factors, one of them being unfavorable climatic conditions for crop cultivation, labor issues, or the spread of disease in the trees.

Usually the older rubber tree is used for rubber extraction as the younger ones contain a larger amount of resin. Also, the quality of the latex obtained from the trees can be judged from factors like the amount of rainfall the cultivation area has received in a particular season, and the location of the trees. Greater amount of rainfall can lead

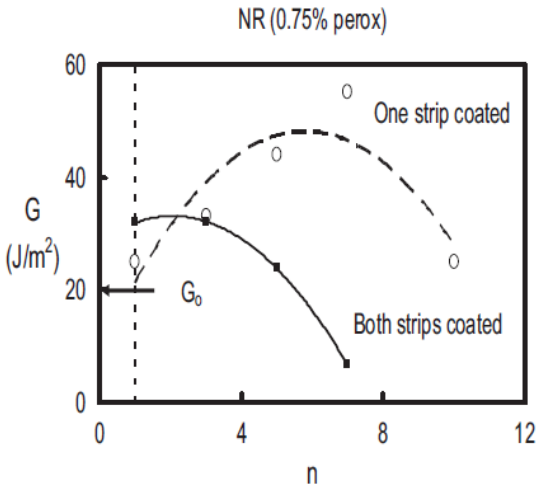

Figure 2.8: Adhesion strengths for both cases of single and both natural rubber layers coated with carbon black. "n" signifies increasing numbers of carbon black layers applied to the surfaces [42]

to a more watery latex, and the lack of rainfall can cause the opposite, which can make latex extraction difficult. The extraction process is done by applying a series of cuts on the trees outer bark so that the latex flows down along the incisions and into a container placed below, as shown in Figure 2.6 [38]. The latex needs to be collected prior to coagulation on the bark. Once extracted, the latex emulsion is processed by various coagulation methods to extract the rubber globules. Some of these, as mentioned in the text by Brown are: spontaneous coagulation, dilution of latex with water and allowing it to stand, dilution of latex with water and subsequent creaming, centrifugal methods, action of heat, or action of acid/salts reagents. After drying and smoking (for improved strength), the rubber bales are prepared for shipment.

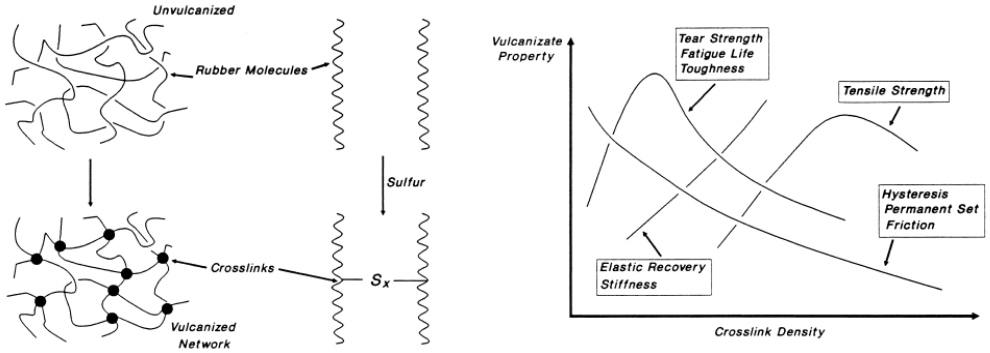

Figure 2.9: A schematic of the polymeric cross-link structure in the rubber, and a graph showing the change in rubber properties with rubber density [33]

Due to its high importance as an incomparable rubber with several mechanical and tribological properties superior to modern synthetic rubbers, including superior impact resistance, green strength and strain induced crystallization [39], it is imperative that the production for natural rubber is highly regulated and controlled in order to sustain continuous production. Recent efforts to develop or cultivate alternate natural sources of the rubber stem from several factors, some of them being spread of diseases like the South American Leaf Blight which can destroy Heavea Brasiliensis crops, excessive labor costs and no possible extraction mechanization process, and increased cases of allergy to protein containing natural rubber [40]. However, there are still several hurdles that need to be crossed in order to fully utilize alternate natural sources and realize their full potential, either by using their unique latex as it is, or by creating genetically modified crops of rubber producing trees that could

provide custom made properties to the end product.

2.3.1 Particle Surface Chemistry

The principal monomer that constitutes natural rubber is isoprene, C_5H_8, present in the latex as cis-1,4-polyisoprene. Recent nanostructure investigation of the surface of freshly tapped natural rubber latex particles done by Nawamawat et al reveals the core-shell structure of the particle with hydrophobic polyisoprene in the center, and a mixed 20 nanometer thick layer of over 80% proteins, with the rest being phospholipids [41]. Using AFM and confocal fluorescence microscopy, they were able to determine that stabilization is mainly due to the charges of the proteins on the particle surface, which itself is around 0.1 – 0.2 micrometers in size. The previous and new model of the particle surface structure are shown in Figure 2.7.

2.3.2 Natural Rubber – Carbon Black Interaction

As previously stated, carbon black aggregates uniformly dispersed in the polymer matrix imparts superior mechanical properties to the composite and makes it of use in applications requiring tremendous amounts of wear, vibration isolation, acoustic damping, etc. In order to maximize these properties, it is important that the adhesion between the carbon black particles and the rubber is reasonably good. Smaller carbon black particles, which are generally referred to as reinforcing particles, are ideal for enhancing mechanical properties due to higher surface area, and eventual increased adhesion of the polymer chains to the particles. A stronger adhesion would imply restriction of movement to polymer chains adjacent to those adsorbed on the carbon black particle surface, thus restricting the free polymeric flow. Additional natural rubber strain induced crystallization can impart properties unmatched by various synthetic rubbers.

Adhesion studies between carbon black and various lightly cross-linked elastomers was done by Nah et al, and their results showed that adding a layer of carbon black between two layers of the same rubber material increased adhesion as compared to self-adhesion when there was no carbon black layer [42]. However, increasing the number of layers between the polymer layers caused a decrease in peel strength, as is evident for peroxide cross-linked natural rubber from Figure 2.8, and it was also found out that natural rubber had a greater adhesion with carbon black owing to its low self-adhesion. Their conclusions are based on lightly cross-linked rubbers, and further work has been recommended for fully vulcanized rubbers. Adhesion is affected during different types of loading, and in a loading-unloading scenario viscoelastic phenomenon known as *hysteresis* is exhibited by the composite due to the breakdown of the carbon black aggregates, and due to particle-polymer debonding

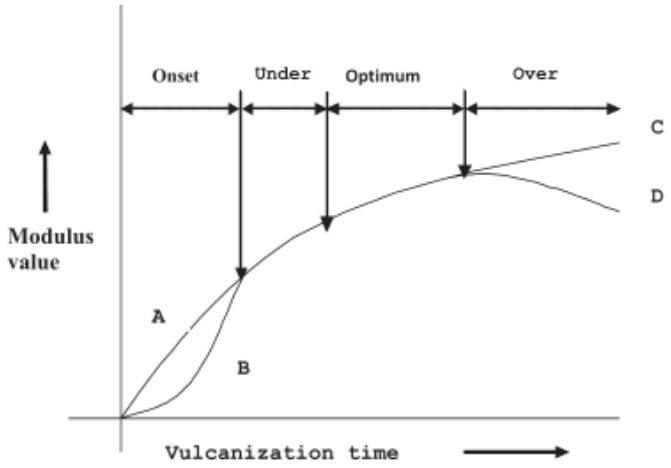

Figure 2.10: The different stages of vulcanization. Over-vulcanization can result in an increase, decrease, or no change in modulus with time, and it generally depends on vulcanization chemistry and the type of chemicals employed [45].

[43]. A temperature increase in carbon black filled polymers will cause restricted movement of the chains and this would contribute to a significant increase in time-dependent behavior.

2.3.4 Vulcanization Characteristics

To put the rubber to any good mechanical use, it needs to be put through a high temperature and pressure process known as *vulcanization*, in which the loose

polymeric network of the highly viscous rubber gum is restrained by poly-sulfidic or mono-sulfidic linkages, commonly referred to as *cross-links*, which impart superior elasticity and reduces the sticky gum behavior. In an unvulcanized rubber, the entanglement of high molecular weight rubber molecules is solely responsible for any retractile force to resist permanent deformation. Said to have been accidentally discovered by Charles Goodyear in 1841 when he was heating natural rubber with sulfur, this process has become an industry standard in manufacturing important industrial and every day rubber items which need to undergo significant amounts of wear and tear and structural deformation. Different vulcanization agents other than sulfur can result in different types of cross-links produced, with naturally varying mechanical characteristics based on type of cross-link and the density of the cross-linking. A two-stage vulcanization process used on strain-induced crystallizing rubber like natural rubber can significantly increase tensile strength, reduction in fatigue crack growth, anisotropic network structure due to the strain induced vulcanization, and strain energy density [44]. Kaang et al were able to create these superior double network dicumyl peroxide processed natural rubber vulcanizates by first creating a partially vulcanized network at a particular temperature and pressure, and then applying a strain before doing the final vulcanization in the oven.

During the rubber product formation process, the ingredients have to be dispersed properly initially in order to achieve uniform material properties. This has to be controlled in the compounding process in which the rubber gum is blended with accelerators, foaming agents, and reinforcement materials like carbon black. The mixing rolls have to maintain a certain degree of temperature to facilitate compounding, however if this temperature reaches the vulcanization temperature of the rubber, then *scorching* will occur and further compounding will not be possible because the rubber would have fully vulcanized. In this complex process, it is important that temperatures are properly controlled so that premature scorching does not occur, and that vulcanization only happens in the final forming process. Prior to using the rubber processing, tests are performed to determine the vulcanization characteristics of the rubber by an apparatus called a *Moving Die Rheometer*, or an *Oscillating Die Rheometer*. These rheometers apply a small oscillatory force to the rubber mix in either an enclosed temperature controlled die, or in a container with the

rubber mix and submerged oscillating disc, respectively. Scorching time, and post-cure characteristics are determined which are used for actual rubber processing. Rheometric tests provide viscoelastic properties as well, in which shear modulus, tan-delta are plotted against time, strain and frequency to delineate the various stages of vulcanization. The *cure curve* plotted by the torque against time is the primary result which clearly provides information on an inreased torque as vulcanization progress, and a slight decrease in post-vulcanization, which is known as *reversion*. The elastic storage modulus tends to increase and the loss modulus tends to decrease as vulcanization time progresses. Reversion, a phenomenon most common in natural rubber based compounds, can also be determined from these plots generated by the rheometric experiments.

Usually vulcanization is not done with elemental sulfur alone as the process can take a considerable amount of time. Various accelerators and activators are used to increase process efficiency. The choice of accelerator has evolved over time, with an increasing requirement to use less toxic, stable, and "delayed action" accelerators

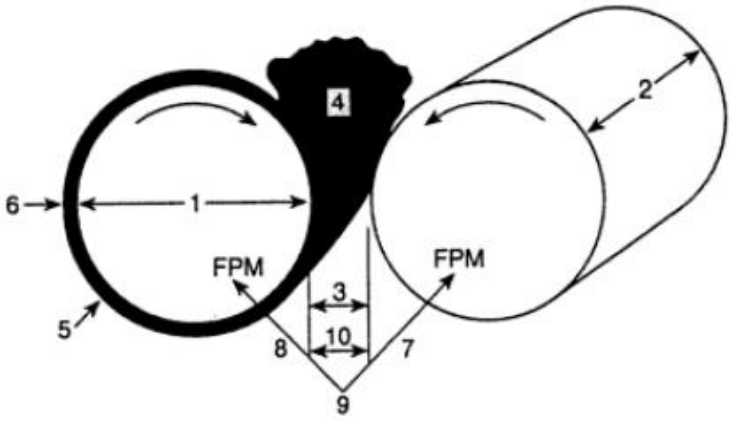

Figure 2.11: Two-roll mill nomenclature [46]

which would also cater for scorch resistance. 2-mercaptobenzothiazole (MBT) and 2-benzothiazole di-sulfide (MBTS) were the first delayed action accelerators used, and are still in wide use today. ZnO and fatty acid like stearic acid are used as activators. The structures of the active sulfurating species formed during the reaction of the accelerator with sulfur is different from the one in which ZnO and stearic acid are used. These active sulfurating species which are basically accelerator polysulfides act

as facilitators for the cross-linking process to occur.

The cross-linking of an elastomer can be done in three general stages [45]:

- Induction period
  1. Gradual thickening with no measurable cross-linking.
  2. This part determines safety against scorching.
- Onset of vulcanization
  1. This is the important part where essential material properties for the final product are developed.
  2. These properties can be achieved by observing the *optimum cure-time.*
- Reversion (over-cure)
  1. Reduction in essential properties like hardness, modulus and tensile strength.
  2. For thicker products, the surface can get over-cured while the core is still in the vulcanization phase.

The use of accelerated vulcanization systems thus provide several advantages which include reduction in the cure time to make the process more economical, cure temperature reduction, reduction in the amount of organic sulfur, improvement in properties with multiple accelerators which facilitate each other, broad plateau in stress heating time curve [45].

2.4 Foam Synthesis and Auxetication

Natural rubber based auxetic foam synthesis has not been explore hitherto by researchers, and the focus has largely been on polyurethane auxetic foam synthesis, its mechanical characterization, and several numerical simulation studies from various aspects of foam mechanical behavior. Initially foam synthesis for natural rubber will be studied here in light of previous research done on the same, and then the work done for auxetic foam synthesis for polyurethane foam will be studied to lay the basic foundation for understanding a generally accepted method for synthesis of auxetic polymeric materials.

2.4.1 Rubber Processing

Prior to reviewing the intricacies of foam synthesis it is imperative that the

fundamentals of processing a basic rubber compound be considered first. Though the foaming agent along with the accelerators, activators, and reinforcements is added during the mixing process, various temperature and time considerations make rubber foaming an entirely separate area of study.

The synthesis of this type of rubber composite (with carbon black as the reinforcement) requires that the constituents be uniformly distributed in order for material homogeneity to establish later on in the compounding process. Unlike the manufacture of other composite materials like laminates, the mixing process requires that the full rheological properties of the foam be understood completely prior to initiating the mixing. This would help to establish the scorch times, the ideal foaming temperature, decomposition temperature of the chemical blowing agent, ideal rubber viscosity for dispersing the carbon black reinforcement, etc. Over time, several mixing techniques have been developed, with their choice based on the constituents employed, the processing conditions employed, and the basic geometry of the final product required. Despite the variations in the mastication and mixing method, where mastication basically refers to the breaking up of the ingredient agglomerates and their resultant dispersion in the mix, the fundamental factors that make up the rubber mixing process is the accurate control of overall processing temperature, the sequence in which the ingredients are added, and a possible requirement for mixing in multiple stages.

Several mixing modes are two-roll milling, internal batch mixing, continuous mixers, extruders. Each has its own mixing characteristics, however two-roll milling will be the focus here as that is the mixing method employed for the synthesis of natural rubber foams in this study.

The two-roll mill basically employs two large metallic rolls (and comparatively smaller ones in a laboratory setting) between which the rubber mix is masticated. The gap between these temperature controlled rolls is monitored and can be varied to accommodate various types of elastomer consistencies. Usually when the rubber is first placed over the gap between the two rolls, it gradually starts to adhere to one roll as time progresses due to temperature increase and adhesion to the roll surface. Repeated cycling of the rubber between the rolls alters its consistency and makes it useful for addition of various powdery constituents. After a certain time, all

the ingredients are added in the right order. The order is important since it is related to the individual dispersibility or decomposition properties. If, for example, a foaming agent is added earlier than its scheduled addition time, it might decompose earlier too due to exposure to more temperature, and would render the material useless. Carbon black addition will also depend on the viscosity of the rubber mix, where a higher viscosity providing a better reinforcement dispersion.

Referring to the a schematic of the two-roll mill system taken from the text by Grossman [46], the various important areas in the two-roll system are (1) the diameter of the roll, (2) the face length which is basically the length of the roll, (3) the roll gap which is an important variable to control processing conditions, (4) the bank size which refers to the amount of the rubber mix placed between the two rolls, (5) the banded roll which is basically the roll over which the rubber has adhered to, (6) the roll on the operators side, (7) the roll whose speed is relatively slower than the other, (8) the relatively faster roll, (9) the speed ratio between the rolls, and (10) the resultant separating force generated by the material between the two rolls.

The shearing force generated causes the breakdown of the agglomerates and promotes better particle dispersion. The mixing process can result in a temperature increase which can cause problems like premature vulcanization if the temperature exceeds a particular limit, however that can be controlled by varying the distance between the rolls in order to reduce the temperature resulting from excessive friction. This process thus allows superior temperature control at the cost of factors like more exposure to surrounding dust, long mixing procedures and operator expertise. It is still a more commonly used mixing method as compared to the internal batch mixer. A common laboratory mixer is provided by Brabender by the trade name *Brabender Polymix* which allows the user to control all the above mentioned factors.

The mixed rubber is then allowed to rest for around 24 hours prior to foaming and vulcanization. After this aging period has elapsed, the masticated rubber is subjected to pressure and high temperature in a hydraulic press to prepare the final product of a required shape and size. During this process, the chemical blowing agent undergoes decomposition, resulting in nucleation of bubbles throughout the rubber matrix, depending on how well the blowing agent was dispersed during the mixing / mastication process. Some of the important factors to keep in consideration when

selecting chemical blowing agents are: (a) the gas should release when the polymer is being processed, (b) the amount of gas release and rate of release should be controllable, (c) the end product should not be affected by any blowing agent residue or the gases generated, (d) the products should not react with other constituents of the mix which could result in product degradation and evolution of undesirable products, and, (e) the tools used for processing should not be affected by the chemical blowing agent and its products, for example, corrosion should not occur [47]. Various studies for natural rubber foaming have employed different kinds of chemical blowing agents. Kim et al have used DPT (N,N-dinitroso pentamethylene tetramine) chemical foaming agent accelerated by Cellex-A, which was used to significantly decrease the decomposition temperature of DPT [48]. The decomposition temperature was reduced to 138^{o}C from 206^{o}C. The reason efforts are made to decrease the decomposition temperature for chemical blowing agents (CBA) is that the decomposition temperature should not come too close to the curing temperature, otherwise incomplete foaming could occur and the cellular properties would not be homogeneous. Research on chlorinated polyethylene foams done by Zhang et al also lowers the decomposition temperature of *azodicarbonamide*, which is a very commonly used chemical blowing agent, by adding zinc stearate (ZnSt), and the drop was from about 200^{o}C to 160^{o}C, with the optimal curing temperature of chlorinated polyethylene identified as 170^{o}C [49]. Ariff et al used the inorganic sodium bicarbonate as a blowing agent for synthesis of natural rubber foams, with the decomposition temperature at around 145-150^{o}C [50]. Similar research was done by Najib et. al. in which acoustic damping properties were improved by controlling the foaming temperature with sodium bicarbonate as blowing agent [51]. So depending on the end properties, the processing environment and the other constituents in the mix, the proper blowing agent has to be selected to establish compatibility with all aspects of the foam synthesis.

The foaming and vulcanization is done in an electric hydraulic press which applies temperature and pressure to the mix for a certain period of time until optimum curing is achieved. Different foaming pressures yield different results, as was identified by Kim et al in their work on natural rubber foams [48]. Different curing temperatures also yield different properties, including a reduction in tensile properties

and elongation and break, and varying foaming temperatures affect curing characteristics [18]. However, varying the carbon black content in both cases of varying pressure and varying temperature conditions gives a variation in general base material mechanical properties, leading to enhanced strength due to increased carbon black content, at the cost of increased foam density due to increased resistance to rubber melt flow during the expansion process due to carbon black particles reinforcement.

2.4.1.1 Possibility of generating an auxetic foam structure during foam formation process

Based on the above general procedures for natural rubber vulcanization and foam formation, an auxetic structure during the foam formation is possible, provided the processing conditions, i.e. the temperature, pressure, and the controlled timed adjustment of the thickness of the foam sheet by applying a tri-axial compression is done to create the ideal auxetic foam structure. Due to the limitation in the process employed to manufacture standard vulcanized rubber or rubber foam sheets, accurately controlling the thickness of the foam sheet using conventional die compression means would not be possible since the die has a fixed cavity size. However, an alternate method of using a specially designed die which would allow mid-process thickness variation of the foam would need to be designed. This would allow adjusting the die cavity dimensions during the process either by employing a mechanism that would have movable die walls. This sort of mechanism would allow the top wall of the die to slide down in order to reduce the dimension of the die cavity, thus causing foam tri-axial compression, resulting in an auxetic structure.

More details about this proposed auxetic foam formation procedure would be discussed in the next chapter.

2.5 Elastomer Mechanical Behavior Simulation: Hyperelastic Behavior

Most elastomers exhibit a behavior known as *Hyperelasticity*, which is characterized by extremely high elongations and a distinct non-linear behavior on the stress-strain curves. This behavior is typically exhibited by filled rubbers, and the

content of the carbon reinforcements effects the loading-unloading curves. Considerable amount of research is done on filled natural rubber hyperelastic behavior, particularly for finite element analysis for damping, high deformation, and other non-linear behavior. Various material models have been formulated which can be used in finite element analysis software for fitting with experimentally obtained data.

Hyperelasticity is a path independent behavior, that is, as has been explained in the text by Bonnet and Wood, that the work done by the stresses during a deformation process is dependent of the initial state and the final state [52]. The behavior of the elastomeric material can be defined by a *strain energy density function*, which allows one to determine the stress-strain relationships. Basically, the strain energy density is the area under the stress-strain diagram for the material under consideration, and can me mathematically represented as:

$$u = \frac{U}{V} = \int_0^{\varepsilon_1} \sigma_x \, d\varepsilon_x \qquad (2.2)$$

Where, U = strain energy, V = volume, σ^x = stress, ε^x = strain.

The principal features of a nonlinear elastic material, as defined in the technical report *Hyperelastic Material Modeling* [36] by Garcia et. al. Are:

1. Non-linear large deformation analyses
2. No permanent deformations (elastic)
3. Lacks stress-strain proportionality
4. Total stress-strain relation derived from strain energy function *W.*

Several hyperelastic material models have been developed, some of which are Mooney-Rivlin, neo-Hookean, Ogden, and Arruda-Boyce. They are generally expressed as a function of the strain invariants I_1, I_2, I_3, or in terms of the principal stretches of the strain tensor [53]. Several hyperelastic constitutive relations with brief explanations are given in Table 2.2. A detail explanation and comparison of the models themselves is beyond the scope of this text. The models are in-built into the ANSYS finite element software, and direct input of the experimentally obtained stress-strain data is needed for curve-fitting to any suitable material model.

Table 2.2: Several equations for hyperelastic material models are used to simulate the mechanical behavior of elastomeric materials.

Model Name	Equation	Comments
Mooney-Rivlin	$W(I_1, I_2) = \sum_{ij=0}^{n\to\infty} c_{ij}(I_1-3)^i(I_2-3)^j,$	This is an infinite series where c_{ij} are constants. Generally a two parameter model is used.
Neo-Hookean	$W(I_1) = c_{10}\,(I_1-3)\,.$	A relatively simpler model as compared to the Mooney-Rivlin model with only one parameter.
Ogden	$W(\lambda_1,\lambda_2,\lambda_3) = \sum_{r=0}^{n\to\infty} \frac{\mu_r}{\alpha_r}(\lambda_1^{\alpha_r}+\lambda_2^{\alpha_r}+\lambda_3^{\alpha_r}-3),$	Developed by Ogden for large deformation incompressible behavior of rubber-like solids. Principal stretches being used instead of invariants.
Yeoh	$W(I_1) = \sum_{n=1}^{i} c_{i0}\,(I_1-3)^i\,.$	Used for incompressible and compressible rubbers. For compressible rubbers, the I_3 invariant is used.
Arruda-Boyce	$W(I_1) = G\left[\frac{1}{2}(I_1-3)+\frac{1}{20N}(I_1^2-9)+\frac{11}{1050N^2}(I_1^3-27)\right] + G\left[\frac{19}{7000N^3}(I_1^4-81)+\frac{519}{673750N^4}(I_1^5-243)\right]+\ldots$	Also known as the eight-chain model because of the nature of the representative model used to describe it.
Gent	$W(I_1) = \frac{-\mu}{2}I_m\,\ln\left[1-\frac{I_1-3}{I_m}\right].$	Strain energy density is a measure of the first strain invariant.
Blatz-Ko	$W(J_1,J_2,J_3) = \frac{\mu f}{2}\left[J_1-3+\frac{1-2\nu}{\nu}\left\{J_3^{-2\nu/(1-2\nu)}-1\right\}\right] + \frac{\mu(1-f)}{2}\left[J_2-3+\frac{1-2\nu}{\nu}\left\{J_3^{2\nu/(1-2\nu)}-1\right\}\right]$	Suitable for foam type hyperelastic materials. Incompressibility is not assumed.

In order to completely characterize a hyperelastic material, several mechanical tests need to be performed. The more the tests, the higher the accuracy of the final model. But usually for common applications a uni-axial test can suffice. However bi-axial tension and planar shear tests can provide information overlooked by an ordinary uni-axial tensile test.

2.6 Elastomer Mechanical Behavior Simulation: Viscoelasticity

Another aspect of polymeric materials that needs to be taken into account for a well rounded mechanical behavior simulation is viscoelastic behavior, which basically implies a time dependent behavior of the material under any conceivable mechanical loading condition. A viscoelastic material has both a recoverable elastic part, and a nonrecoverable viscous part. So generally, in order to reasonably describe the mechanical behavior of an elastomeric substance, both hyperelastic and viscoelastic properties need to be determined up to a certain degree of accuracy required by the experiment.

The study of viscoelasticity is a fairly complex subject with various mechanical loading and temperature variation effects altering the behavior of the material in different situations. Several models have been developed to describe the time dependent response of materials, which will be gone through briefly in this text, along with the finite element application of the models and constitutive relations.

Polymeric viscoelasticity is characterized by stress relaxation, creep, and temperature dependent response. Due to the weak inter-chain van der Waals forces in elastomers and thermoplastics, the chains are able to slide past each other more easily than the tightly bound atoms in non-polymeric materials. This allows the elastomers or polymers to show creep behavior at even lower temperatures [54]. Stress relaxation implies a reduction in the developed stress in a material due to a constant strain applied, whereas creep refers to variation in strain due to a constant stress being applied. These are usually explained with the help of spring-dashpot models, where a spring and a dashpot connected in series or parallel with each other, which explain the stress-relaxation and creep behavior, respectively. The Maxwell model, which is the

series model, is more applicable to a stress-relaxation scenario, whereas the Voigt model, which is the parallel model, is more applicable to creep situations, as is explained by the predicted stress-time and strain-time graphs shown in Figure 2.12.

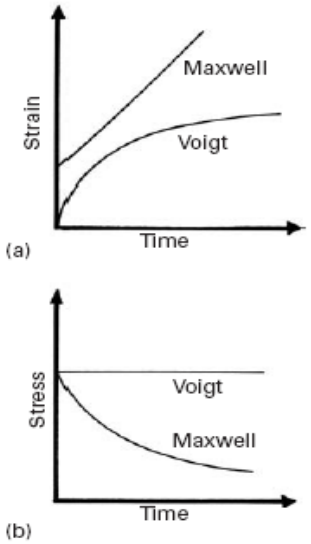

Figure 2.12: The strain-time (a) and stress-time (b) graphs showing the difference of applicability of the Maxwell and Voigt models to a constant stress and constant strain situation [54].

Temperature dependence of viscoelasticity on the behavior of the material implies variations in the stress-relaxation or creep with time with varying the temperature conditions. A *thermorheologically simple* (TRS) material is one which shows the same viscoelastic behavior are high temperature and low strain rate conditions, and vice versa. For example, in a typical impact situation, an elastomer might tend to be extremely hard during initial contact due to the high strain rate and very small relaxation time available, and at sub-zero temperatures where the elastomeric substance freezes (which is defined as the *glass transition* temperature), a similar viscoelastic behavior would be exhibited. Usually a series of curves obtained at different temperatures is plotted on a log graph by using certain principles of shifts, which allow the curves to blend into each other and form one master curve. There are various advantages of using a master curve, one of them being able to study the material under a few temperature conditions and predict the behavior at other un-tested temperature conditions by using the curve. Temperature dependence on

viscoelastic behavior, however, has not been the focus of this research, so it will not be delved into further.

2.6.1 Prony Series

The Prony series is also referred to as the Generalized Maxwell model, which basically is various spring-dashpot series assemblies connected in parallel. From a conceptual point of view, it has been explained in various texts on polymeric viscoelasticity that polymers have a haphazard distribution and orientation of the polymeric chains in the material, and it is very likely that the relaxation time one particular location in the material might differ from another location due to this inhomogeneity. The Prony series caters well for this inhomogeneity by introducing several relaxation times and moduli in the series. Depending on how accurate the results are required, several parameters in the Prony series can be chosen to represent the viscoelastic behavior of the polymeric substance in its entirety.

The time dependent response in viscoelastic materials is separated into volumetric and deviatoric terms [55], as shown in the equation below. This is the constitutive equation for an isotropic viscoelastic material.

$$\sigma(t) = \int_0^t K(t-t')\frac{d\epsilon_v}{dt'}dt' + \int_0^t 2G(t-t')\frac{d\epsilon_d}{dt'}dt' \qquad (2.3)$$

The kernel functions are represented in terms of the Prony series, which are as under:

$$\begin{aligned} G(\tau) &= G_0\left[\alpha_\infty^G + \sum_{i=1}^{n_G}\alpha_i^G e^{-\frac{\tau}{\tau_i^G}}\right] \\ K(\tau) &= K_0\left[\alpha_\infty^K + \sum_{j=1}^{n_K}\alpha_j^K e^{-\frac{\tau}{\tau_j^K}}\right] \end{aligned} \qquad (2.4)$$

The alpha terms denote the relative moduli for the deviatoric and volumetric components of the constitutive relation, and that is required as an input for ANSYS finite element software, in addition to the relaxation times. For cases where sufficient viscoelastic data is not available, only the deviatoric component of the relation should be used.

CHAPTER 3

EXPERIMENTAL AND SIMULATION SETUP

A combination of experimental and computer simulation work has been done to analyze the mechanical behavior of natural rubber based auxetic cellular structures. The intent is to simulate the behavior of auxetic micro-cellular structures using the mechanical properties obtained from vulcanized natural rubber in the form of its hyperelastic and viscoelastic behavior. The recipe used for the formation of the vulcanized natural rubber sheets has previously been used for the formation of natural rubber based conventional (non-auxetic foams). The reason the use a recipe for development of the natural rubber has been to approximate the natural rubber state in its vulcanized cellular form. Simulation was largely done on finite element analysis software ANSYS, with additional modeling support from surface modeling tool Rhinoceros. Various structural configurations, loading scenarios, cellular structures have been analyzed using the base material's hyperelastic properties, which are then used in conjunction with the base material viscoelastic behavior obtained from stress relaxation data to develop a simulation for a proposed application of the cellular auxetic material.

3.1 Vulcanized Natural Rubber Sheet Synthesis

Vulcanized natural rubber sheets were developed at International Polymer Industries, Islamabad, using conventional rubber products synthesis technology being

widely used in the local industry. The employment of standard vulcanization equipment as opposed to a laboratory based setting was preferred since the intent has also been to analyze the behavior of vulcanized rubber used commonly for various automotive, sports, and other defense related applications.

A set of one 2mm thick and 6mm thick sheets were made using a standard 6 x 6 inch die for four different loadings of carbon black, i.e., 6%, 12%, 18%, and 24%. The steam operated press was used to vulcanize the 8 rubber sheets using a pressure of around 3 bar for a duration of 30 minutes. Prior to the vulcanization, the compounding was carried out on a small mixer using the recipe shown in Table 1. The order of addition of ingredients for the compounding process was: rubber, MBT, TMT, ZnO, Carbon Black, Stearic Acid, Sulphur. Vulcanization was carried out about 30 minutes after the compounding process in a pre-heated steam press.

Table 3.1: Formulations of natural rubber compounds

Ingredients (phr)	NRV-1	NRV-2	NRV-3	NRV-4
SMR (Standard Malaysian Rubber)	100	100	100	100
Stearic Acid	2.5	2.5	2.5	2.5
ZnO (Zinc Oxide)	5	5	5	5
Carbon Black	6	12	18	24
P. Oil (Paraffin)	27.5	27.5	27.5	27.5
MBTZ (Mercaptobenzothiazole)	1.2	1.2	1.2	1.2
TMT (Tetramethylthiuram)	0.1	0.1	0.1	0.1
Sulfur	2	2	2	2

3.2 Characterization

3.2.1 Mechanical characterization

The purpose of characterizing the prepared vulcanized rubber sheets was to use the mechanical properties obtained for input as material properties in the finite element analysis software. For this purpose two mechanical tests were carried out on the rubber sheets as per ASTM 412C (Standard tests methods for vulcanized rubber and thermoplastic elastomers - Tension), and ASTM D-6147 (Test method for vulcanized rubber and thermoplastic elastomer – Determination of Force Decay (Stress Relaxation) in compression). The uni-axial tensile test and the stress relaxation in compression test were carried out on a UTM (Shimadzu) at room temperature with a tensile and a compressive fixture, respectively. Tensile test samples were cut out from the 2mm thick sheets for each of the carbon black loadings as per the requirement of the ASTM 412C standard, and stress relaxation compression test sheets were cut out from the 6mm thick sheets in the form of 13.5 diameter and 6mm thick cylinders, as per the ASTM 6147 standard. No pre-treatment was done on the samples prior to the mechanical testing.

3.2.2 Scanning Electron Microscopy

Carbon black nanoparticles were viewed under the SEM to determine their size distribution and agglomeration. Dry carbon black and carbon black sonicated in ethanol were both viewed under the SEM, the latter giving less distinct nanoparticles separate from each other in the images.

3.3 Modeling and Simulation

The aim of the finite element simulation has been to characterize the mechanical behavior of cellular auxetic structures for vulcanized natural rubber as base material, using different carbon black loadings. The SEM data obtained from a separate research of natural rubber based foams was used as a reference to determine the approximate cell size that should be used to develop idealized models of a small portion of the foam using surface modeling software Rhinoceros. Several 2D planar

cross-sections of an idealized conventional and auxetic foam structure were developed using the modeling tool, which were then exported as IGES format files to be input into the finite element analysis software.

The SEM micrographs of the natural rubber foams showed varying cell sizes, and the cell size distribution was not easily discernible between the different carbon black loaded foams. An average value of 200 micrometers was chosen to model the cells based on the relatively more spherical and larger cell sizes for the case of a 6% carbon loaded natural rubber foam.

The geometry of the idealized conventional (non-auxetic) foam specimen was designed by arranging an array of 200 micrometer spheres inside a rectangle of dimensions 2mm x 1.5mm. The geometry was two-dimensional in order to save on computation time, and the sample thickness was provided to the finite element analysis software as 0.1 micrometers. This idealized conventional foam geometry was subjected to various deformations, as will be explained later.

3.3.1 Generation of the auxetic structure graphical model

Previous research done on polyurethane based foam auxetication shows that tri-axial compression and subsequent heating up to the softening point of the base polymer, and finally cooling in that compressed state leads to the formation of the re-entrant auxetic cellular structure. However, vulcanized natural rubber does not fall under the category of thermoplastic elastomers and therefore does not have a definite softening temperature which can be used to buckle the walls of the conventional foam to generate an auxetic structure. Thermoset auxetication can be done by a special one-step process which would first allow the foam to expand as per the normal foaming process, and then a slight calculated tri-axial compression should be applied while the rubber is still curing in order to buckle the melt walls while it is still in the curing phase. The process has also been stated in the patent titled *A process for the preparation of auxetic foams* [56]. This process may allow the generation of an auxetic cellular structure for a thermoset like vulcanized rubber, however there are some points that need to be considered while undertaking this manner of synthesis:

- In order to obtain a reasonable negative Poisson's ratio, a large pore size would be required, which can only be achieved by reducing the carbon black content,

or by varying the temperature and pressure conditions. Increasing temperature would reduce the viscosity, and hence allow ease in expansion.

- The standard vulcanization methods employed in the industry for rubber products development or rubber foam development require that a considerable amount of pressure and temperature be applied in a die having fixed dimensions. The idea of applying a tri-axial compression during vulcanization would require specialized manufacturing equipment and dies, thus complicating the over-all procedure for auxetication of vulcanized rubbers.
- Cellular structures in vulcanized natural rubber foams may have several walls already buckled, even though no auxetication method was applied. This is due to the fact that confined foaming results in buckling of the walls, resulting in non-spherical voids and an overall distorted cellular structure.

Whatever the manner of auxetication employed for thermosetting elastomers like vulcanized natural rubber, the final structure needs to be re-entrant, and the degree of auxetication should be suitable for either a compression or tension application.

Two models for the auxetic structure were developed; one for the case of tension, and another for compression. The auxetic structure for compression was moderately re-entrant, whereas the auxetic structure for tension was highly re-entrant. The idealized conventional foam structure was subjected to a compression from the side walls and from the top to first generate a compression application re-entrant structure of dimensions 1.817 x 0.910 mm. For tensile loading cases, the structure was further compressed to result in a higher re-entrant structure with dimensions 1.4 x 0.704 mm. The manner of generating these structures was by standard quasi-static finite element loading. Element selection in the ANSYS software was PLANE183, and the thickness was given as 0.1mm for the geometry under consideration. The experimental stress-strain curves were used to curve-fit hyperelastic material models, as will be discussed later in this chapter. Once the final compressed state for both cases was achieved using the finite element simulation, the structure geometry was traced using Rhinoceros, and then re-input into the ANSYS software for further simulation purposes.

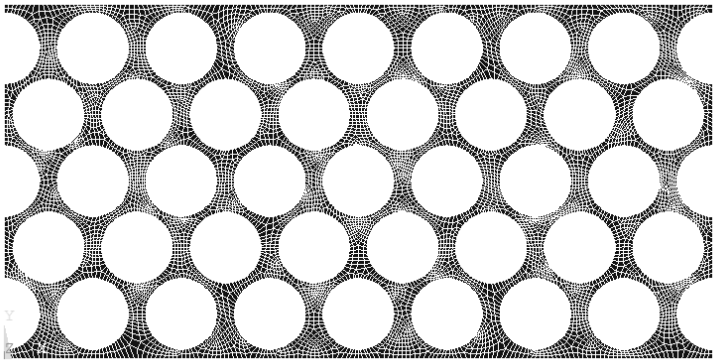

Figure 3.1: Idealized conventional foam model

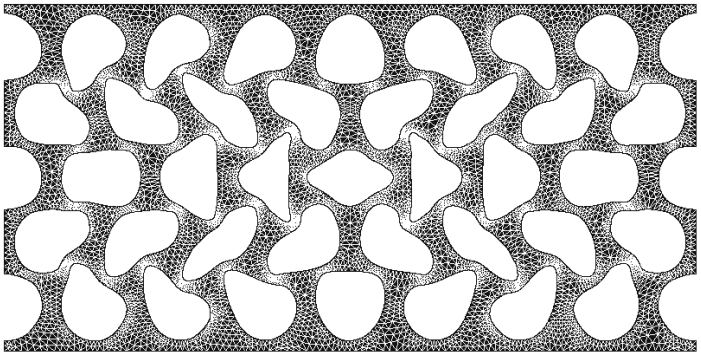

Figure 3.2: Lightly auxeticated structure for compressive applications

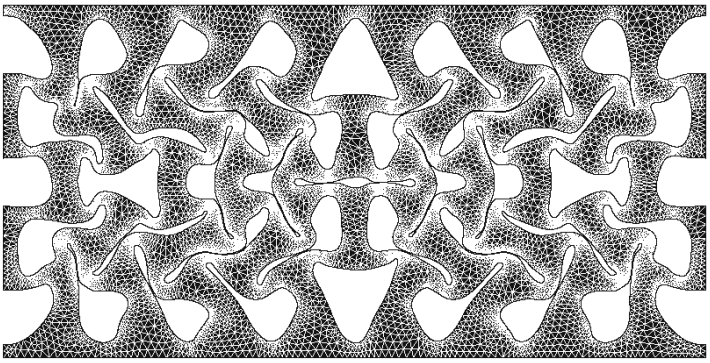

Figure 3.3: Highly auxeticated structure for tensile applications

3.3.2 Hyperelastic Curve Fitting

Curve-fitting was performed via the in-build tool in the ANSYS finite element analysis software. True Stress vs. True Strain graphs were developed from the experimental data, which was then fed to the curve fitting tool. The process was done

using 3 parameters for the Mooney-Rivlin model, which seemed to provide a good fit for the experimental data with a tolerable amount of error. Curve-fitting was done for all four carbon black loaded rubber tensile test experimental data.

3.3.3 Viscoelastic Curve Fitting

Stress-relaxation tests performed on the 6mm thick rubber sheet specimens were used to generate the viscoelastic material model compatible with the hyperelastic model already defined. Three parameters of the Prony series were used to curve-fit, with no parameters for the bulk behavior, and no shift functions involved. Several tweaks had to be made for a reasonable curve fit for this short time duration relaxation. During experimental stress-relaxation testing, the force had to be manually recorded at 5 second intervals for 30 minutes since time recording method in the testing apparatus was not available. The interval was kept as small as possible to detect minute changes in the relaxation behavior. It was observed, however, that the stress relaxation was sudden in the initial few seconds of the start of the experiment, and decreased very gradually later, as will be explained in the results discussions of this text.

3.3.4 Simulation Details

Following list of simulation tests were done, each for the four carbon black loaded specimens:

3.3.4.1 Full auxetic structure lateral pull:

The fully auxeticated structure shown in figure 3 was used in extension simulations, one of them being the lateral pull, in which the structure was uniformly stretched in the direction of its shorter length (Y direction). It was a simulation done using Large Deformation Static setting in ANSYS, which allowed determination of the situation of the structure under uniform quasi-static loading. The purpose of this test was to investigate internal structural changes due to the pull in the lateral direction, which were recorded as nodal displacements and stresses in spreadsheets. Only hyperelastic material model was made, and viscoelastic properties were not

introduced here since those were not the primary intent of investigation in this simulation. The stretch was done sufficiently to bring a noticeable change in the internal structure, without causing any instability during the analysis due to excessively large unwanted deformations or element distortion.

3.3.4.2 Full auxetic structure longitudinal pull:

A similar test was done but in the longitudinal pull direction to assess the behavior of the structure in that particular direction. Again this was done without taking viscoelastic effects into account, and was done for all four types of carbon black loaded specimen experimental data. The stretch was sufficient in the longitudinal direction (X direction) to cause noticeable internal structural changes. The left side of the structure was fully constrained, whereas the right side was pulled a distance of about 4-5 mm in order to induce the stretch in the X direction.

3.3.4.3 Lightly auxeticated structure full compression:

The lightly auxeticated structure was designed for compression related experiments, as shown in figure 2, and it is obvious that none of the cell walls are in any sort of contact with each other. This test was performed by uniformly compressing the top surface of the foam by a displacement of about 0.2mm (in downwards Y direction). Only the bottom surface was fully constrained. This was also done quasi-statically without considering viscoelastic effects. Internal contact pairs were defined for the cell walls since contact was expected for the case of compression simulations.

3.3.4.4 Lightly auxeticated structure cylindrical body contact:

As opposed to the full surface compression simulation, this simulation was done by displacing a cylindrical shaped object of relatively high elastic modulus and Poisson ratio suitable for metals. This was done quasi-statically to observe the structural changes due to contact of a small diameter body, which eventually tries to penetrate the foam. Contact pairs were defined not only for the internal walls of the auxetic structure, but also between the foam structure and the incoming object.

3.3.4.5 Lightly auxeticated structure full compression with viscoelastic properties:

Using both the hyperelastic and viscoelastic material properties defined for the material model, the full compression test was done in order to investigate the effects of the recorded stress-relaxation data for the base rubber material on the auxetic structure. This was done in two load-steps in the ANSYS software. The first load step involved setting an arbitrary time in which the required compression displacement was applied, and was done using pre-stressing conditions in order to save the compressed state for the second load step. The second transient analysis load step then used the compression results from the previous load-step, and by keeping the displacement constant for a duration of 5 seconds, the effects of stress relaxation on the auxetic structure were recorded for all four carbon black loaded specimens. This was a full transient analysis as compared to the static analyses performed earlier. The transient analysis was required to observe the effects of the time dependent properties of the base material on its respective auxetic cellular structure.

CHAPTER 4

RESULTS AND DISCUSSION

4.1 Overview

The experimental results and observations concerning the base material (natural rubber) will be reviewed in detail in this chapter, along with the corresponding auxetic cellular structure simulations, for which all the experimental data for the base material was collected. The simulation data will be reviewed largely in the form of comparative graphs and displacement/stress contours for the models generated. The simulation results would be interpreted to characterize the performance behavior under mechanical loading of cellular natural rubber based idealized auxetic structures.

4.2 Carbon Black SEM

Carbon black nanoparticles were obtained from the general carbon black commercial supply at International Polymer Industries, Islamabad. The company imports the 550 grade carbon black from Iran. Standard SEM micrographs were obtained for the nanoparticles in order to determine the size and agglomeration of the particles in the powder. Images were obtained for the case of dry carbon black, and for carbon black dissolved in ethanol. Carbon black was ultrasonicated in ethanol for about 10-15 minutes before being analyzed in the scanning electron microscope. However, the nature and quality of the images obtained from powder dissolved in ethanol and dry powder were different, with the latter showing more distinct, measurable carbon black agglomerates.

It was observed that the particle sizes ranged from 45-60 nanometers, bringing it approximately equal to the carbon black grade 550. The particles do not appear to be distinct from each other as each particle is associated with agglomerates of varying shapes and sizes. These chunks of agglomerates will eventually serve as reinforcement in the vulcanized rubber, unless some chemical process is included to disperse the nanoparticles in the pre-cure rubber melt.

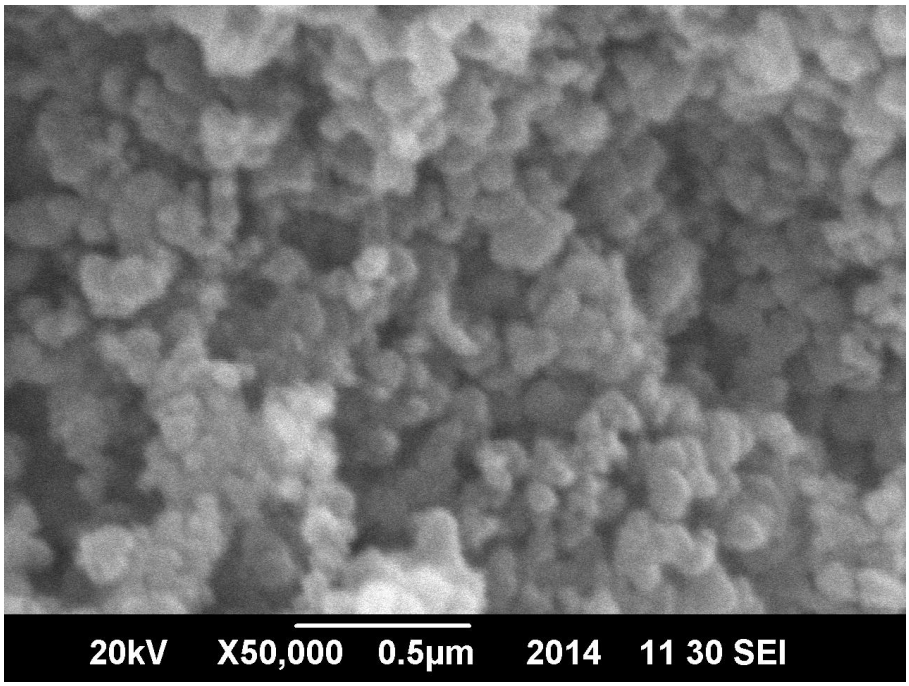

(a)

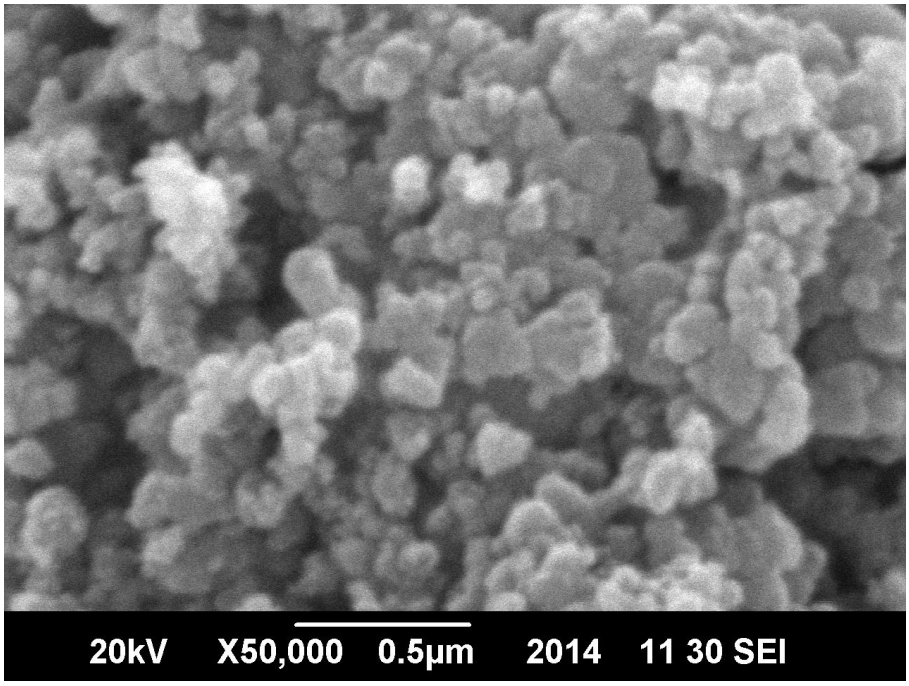

(b)

Figure 4.1: Dry carbon black SEM mirographs at x50,000 magnification show particles and agglomerates clearly.

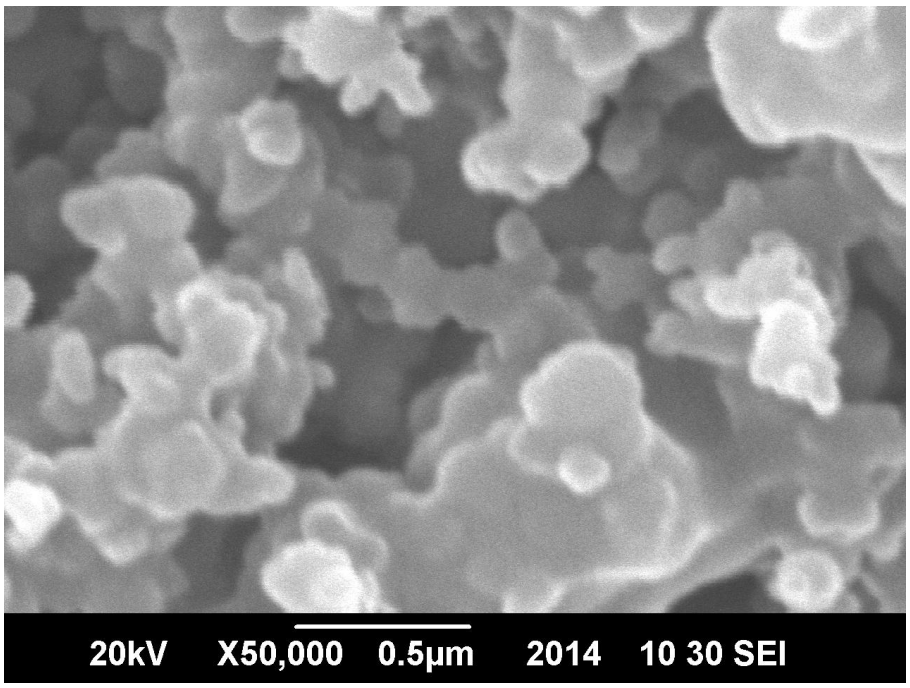

(a)

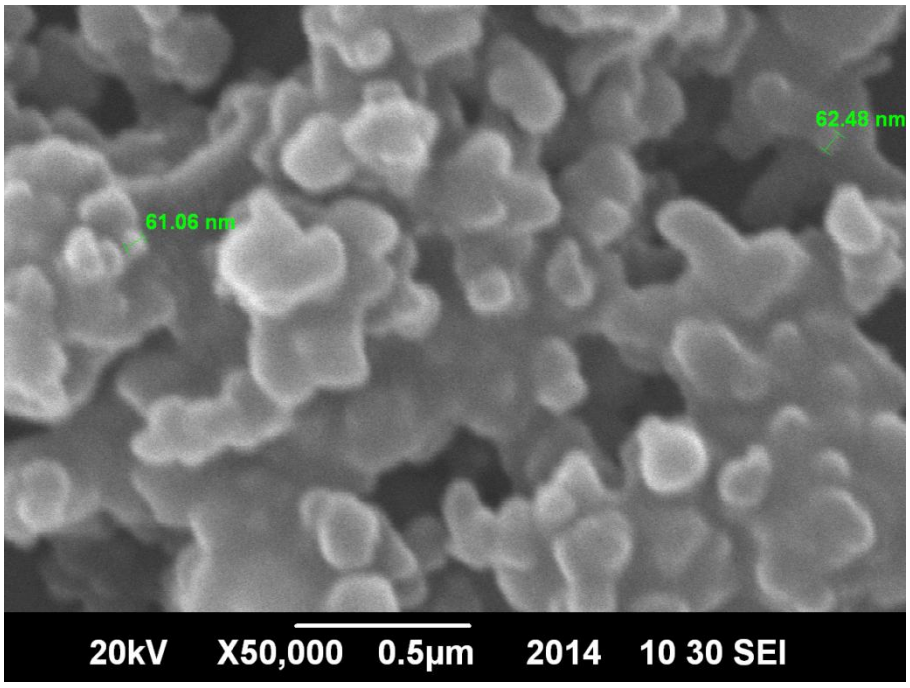

(b)

Figure 4.2: Dry carbon black SEM mirographs at x50,000 sonicated in ethanol do not clearly show particles distinct from each other.

4.3 Tensile tests

Tensile tests performed in accordance with ASTM D412C yielded the results shown in Figure 4.3 for all four varying carbon black loaded specimens.

Minor fluctuations in the curves were observed, but those have been attributed to machine error rather than the inherent property of the material itself. It has been observed that the 6% and 24% carbon black loaded vulcanized natural rubber specimens failed with less elongation as compared to 12% and 18%. This has been attributed to the increased carbon black loading in the case of 24% carbon black, resulting in a relatively less elastic material. However, the initial deformation is more than sufficient to fulfill the primary intent, which would be the examination of minute deflection and stresses in the idealized auxetic simulation models which have been designed at a micrometer scale.

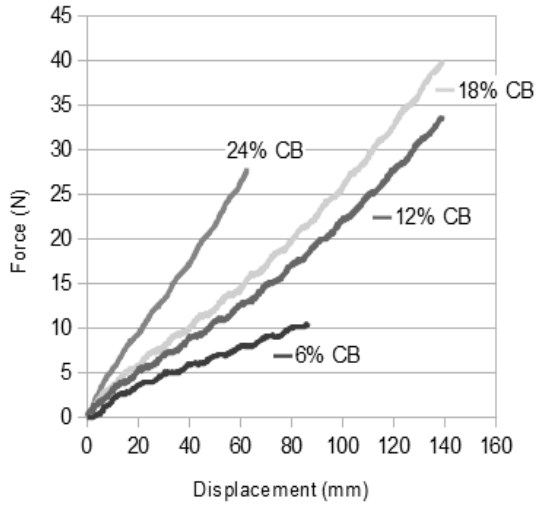

Figure 4.3: ASTM D412C tensile tests for all four carbon black loaded vulcanized rubber specimens.

The load-displacement curves obtained from the tensile tests were converted to Engineering Stress – Engineering Strain curves, as required by the ANSYS

software for hyperelastic material modeling.

4.4 Compression and Stress-Relaxation Tests

Standard compression testing for the rubber specimens was done for samples 6mm thick and 13.5mm in diameter. The actual intent was to record stress relaxation behavior. After a reasonably fast compression up to 25%, the strain was kept constant, and the stress was allowed to relax. Force was recorded at 5 second intervals during the relaxation phase. Figure 4.4 shows the compression curves for all the cases. Notice how close the loading curves for the 12% and 18% CB loaded specimens are. The reason why both of them seem to be so close in their properties can be attributed to the fact that processing conditions can significantly affect the final properties of the vulcanized rubber specimen. Since the synthesis was done in steam pressure based apparatus with some pressure variations during the vulcanization process, such variations are inevitable.

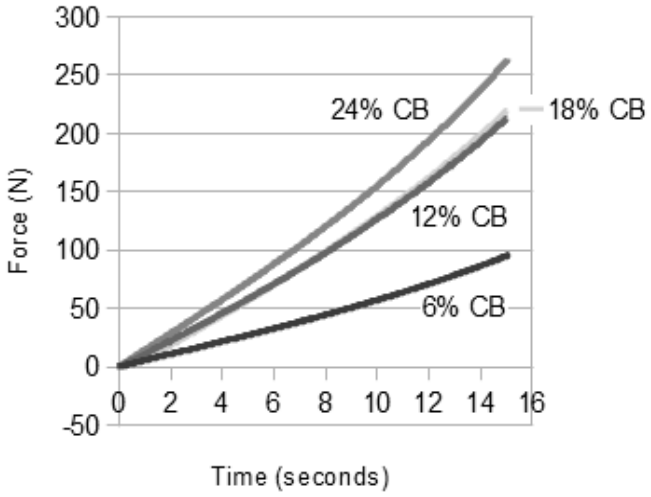

Figure 4.4: Force-Time curves for compressive loading for all cases.

The stress relaxation curves for all the four cases are shown separately in the following series of images shown in Figure 4.5. They have not been super-imposed onto each other for sake of clarity, since the starting force varies from sample to sample. Sudden relaxation takes place during the first few seconds of the stress-relaxation tests for all four cases, and then the relaxation becomes almost linear and less visible. This implies that a large portion of the polymer chain sliding and re-

arrangement takes place under high stress situations, and subsequent relaxations are due to gradual displacement of the polymer chains under less pressure. It is observable that the higher carbon black loaded specimen has a higher rate of relaxation as compared to the lower carbon black loaded specimen, and this has been validated by recent research by Laiarinandrasana et. al. in their simulation based work for filled rubbers [57].

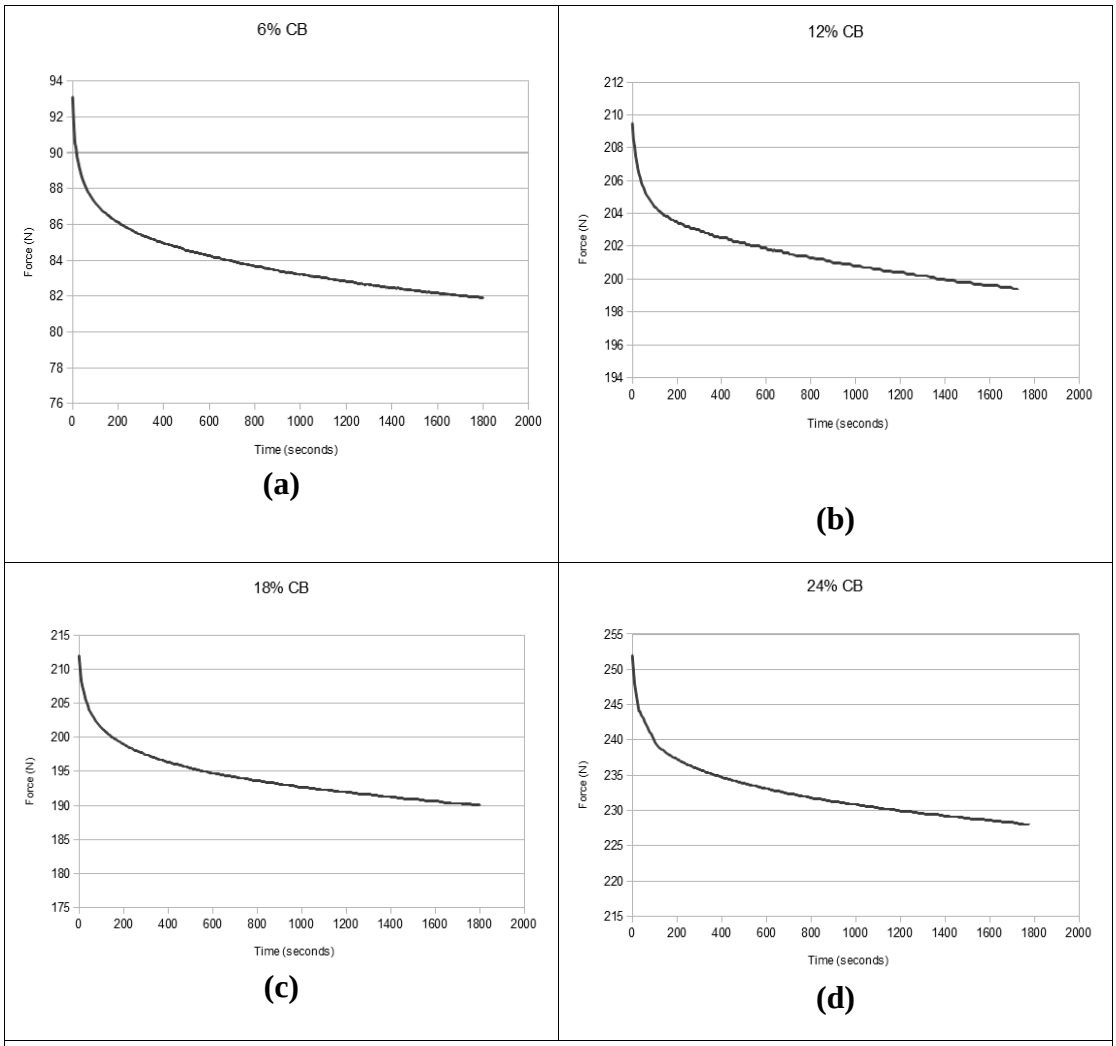

Figure 4.5: Relaxation curves for all carbon black load cases based on an ASTM D-6147 for an approximate 30 minute duration.

4.5 Hyperelastic Curve-Fitting

The Force - Displacement curves obtained from the tensile tests performed on a UTM were converted to Engineering Stress – Engineering Strain curves to be input as experimental data for the curve-fitting process. Due to machine error, minor fluctuations were observed in the curves, which contributed to the small but tolerable error in the curve-fitting process. The Mooney-Rivlin 3-parameter model was used and resulted in reasonable fits for all four carbon black load cases. The Mooney-Rivlin parameters obtained by the curve-fitting the experimental data provided to the software without any tweaking are given in Table 1. The short duration 6% CB curve had prominent fluctuations, and the normalized error was considerable. Normalization was turned off for all cases to get a good match for the entire length of the curve. The curve-fits for all the four cases are shown in Figure 4.6.

Table 4.1: Mooney-Rivlin 3-parameter model material constants

	6% CB	12% CB	18% CB	24% CB
C10	0.132463	0.177917	0.100447	0.212981
C01	-0.028342	-0.063118	0.132516	0.129011
C11	-0.000325	0.008434	0.016084	0.031653
d	0.000000	0.000000	0.000000	0.000000
Residual	0.269352	4.850361	0.597643	0.108842

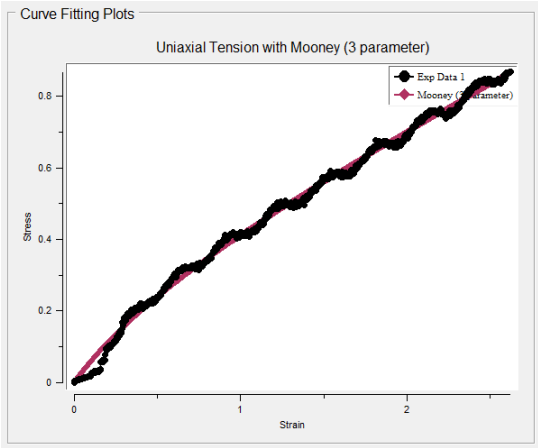

(a) 6% CB Curve Fit

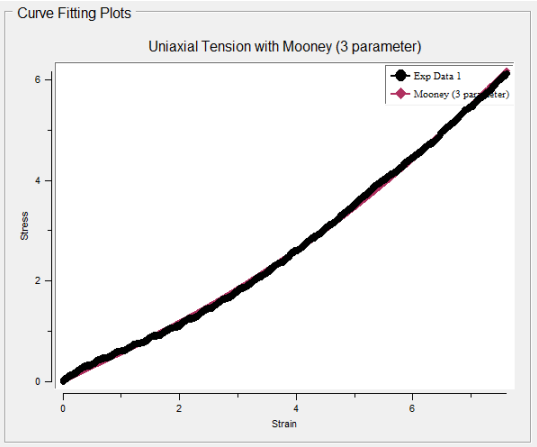

(b) 12% CB Curve Fit

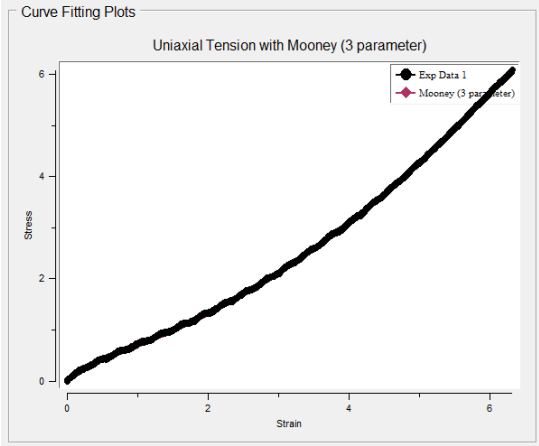

(c) 18% CB Curve Fit

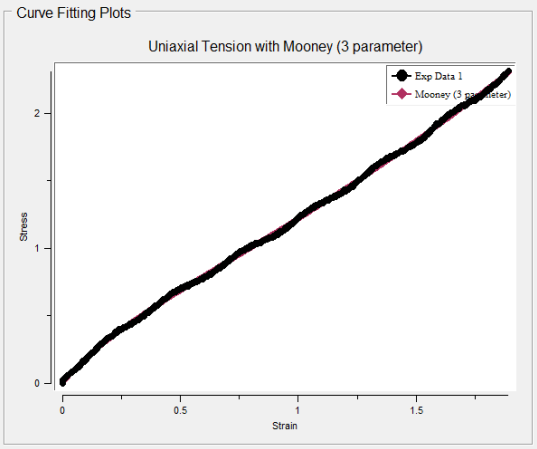

(d) 24% CB Curve Fit

Figure 4.6: Mooney-Rivlin 3-parameter curve fits for all four carbon black load cases. The "Normalized Error" option was turned off for these hyperelastic curve fits to give a better match to the curve, with a relatively less residual error.

4.6 Simulation Runs

The finite element simulations were performed on a 3.1 Gigahertz processor

machine with 4 Gigabytes of RAM. The ANSYS Mechanical APDL software was run for each of the simulation runs using full available system resources. The main focus of the static analyses was to investigate the structural changes in the idealized auxetic model with the applied displacement, and the transient analysis were used to investigate the effects of viscoelasticity on the stress relaxation and consequently the structural changes associated with that relaxation in the models.

4.6.1 Static vertical stretch tests

Keeping in view that the model was based on a small representative portion of the 2mm thick vulcanized rubber sheets, the top and bottom surfaces are the ones experiencing direct contact with the surface of the die. A pull in the foam rise direction should directly influence the material cellular structure and affect the pull surfaces less. Since the structure was fully auxeticated, which means that full tri-axial compression was applied till the internal wall buckled and came into contact with each other, it was observed that a pull in the vertical direction caused the internal "nodes" to displace in the negative (outward) direction first, and after some time the data showed them as moving back inwards. This observed phenomenon is characteristic of negative Poisson ratio auxetic materials, and it's effect has been observed in connection with increased carbon black loading in this research.

Figure 4.7 shows the regions on the idealized auxetic structure which have been observed for all three cases. Region (a) is the surface where the stretching displacement constraint was applied, and 15 location at the top were monitored for Y component of the reaction force. Region (b) identified in Figure 4.7 contains 28 "nodes", which are basically the junctions where various ribs in the cellular structure meet. These nodes remain largely unaffected and have been observed to remain unaffected in terms of deformation during the initial stages of the pull. The X direction displacements of this region were observed to see how the generated auxetic structure would result in a negative Poisson's ratio behavior.

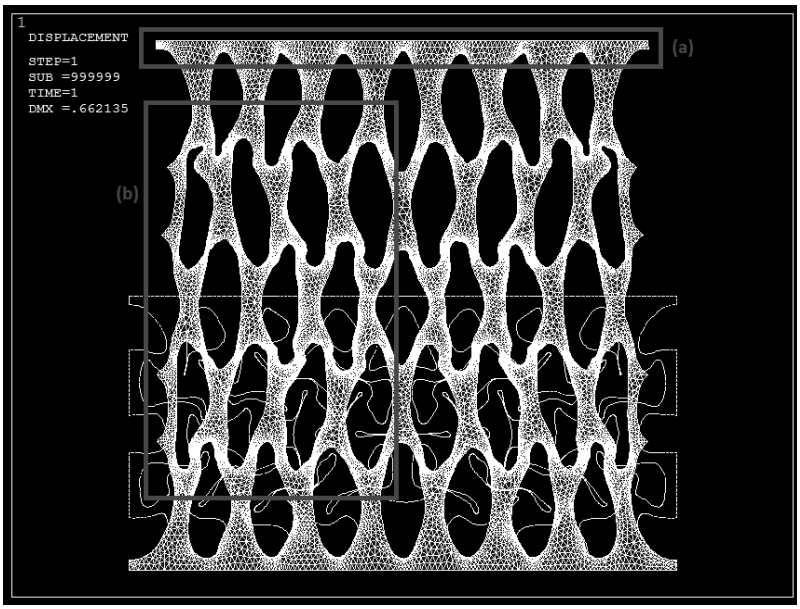

Figure 4.7: The image shows the deformed mesh of the auxetic structure when pulled in the Y direction. Region (a) was analyzed for reaction forces generated, and region (b) was analyzed for "nodes" displacements in the X directions, where the nodes are the regions of the models where the ribs/walls intersect.

The plots shown in Figure 4.8 for all carbon black load cases show structural deformation behavior characteristic of auxetic structures. Although this is an idealized model of an auxetic structure and does not analyze an auxetic structure three-dimensionally, it still provides information on the mechanics of deformation and displacement of various internal points in the cellular structure. The region (b) defined in Figure 4.7 has 8 planes of nodes for which the displacements have been observed in the X direction, relative to the perpendicular Y direction stretch displacement. Figure 4.8 shows the X direction displacement curves for the top “plane” of internal nodes within this region (b) for all four carbon black cases, and Figure 4.9 shows the central plane-4 nodes displacements for the same.

Several direct observations can be made from this basic vertical extension of the auxetic foam structure.

- The negative Poisson's ratio behavior is valid for only a limited extension, beyond which the material behaves more or less like a conventional foam. This is due to the fact that the nodes would have had rotated completely and returned to their un-auxeticated state. The rotation of rigid nodes has been

investigated earlier in the work done by Grima et. al. [29]. Depending on material properties, the nodes may or may not rotate completely.

- The nodes along a plane have a decreasing tendency to displace in the X direction inwards into the cellular structure. This means that the inner most nodes experience least X displacement as compared to the nodes in the outermost exposed portion of the cellular structure. Consequently, this would also imply that the ribs in the inner portion of the cellular structure would not be bearing the same amount of stress as compared to the ribs and walls in the outer exposed portion of the cellular structure.
- The central plane of the cellular structure experiences the most displacement in the X direction, with the outer most node (node 1 on plane 4) experiencing the most displacement. This is due to the fact that the central portion experiences the least restraint and X displacement is limited only by the organization of the cellular structure, and the rigidity of the ribs and walls in the cells.

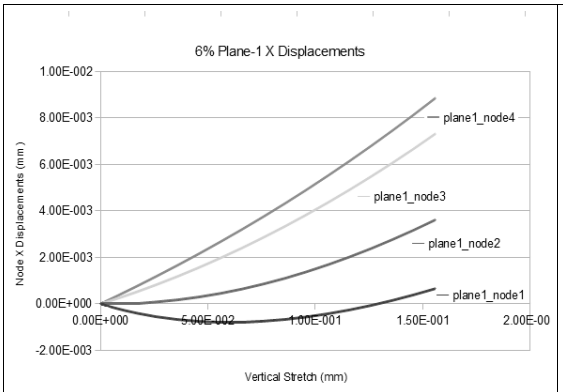

(a)

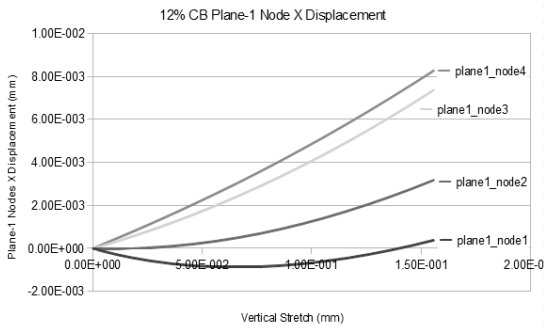

(b)

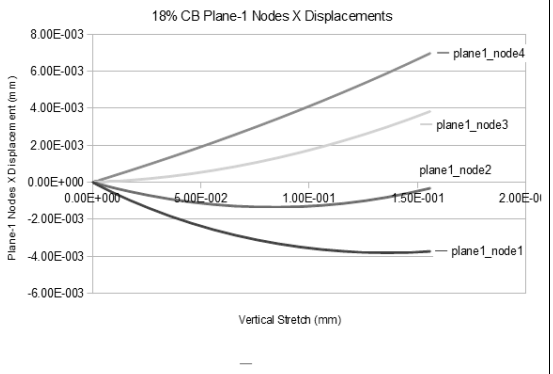

(c)

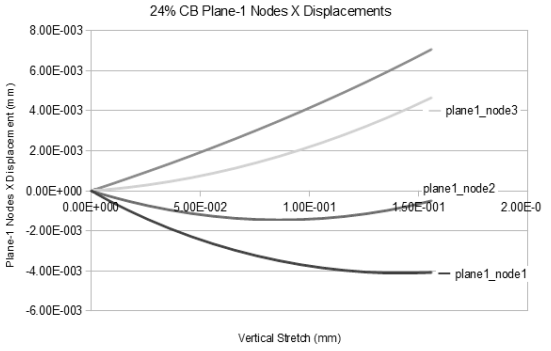

(d)

Figure 4.8: X direction displacements (magnified) for the top plane of internal nodes in all four carbon black load cases. Maximum X direction displacement was achieved by the outermost node on plane-1 for 24% CB loading, shown in (d).

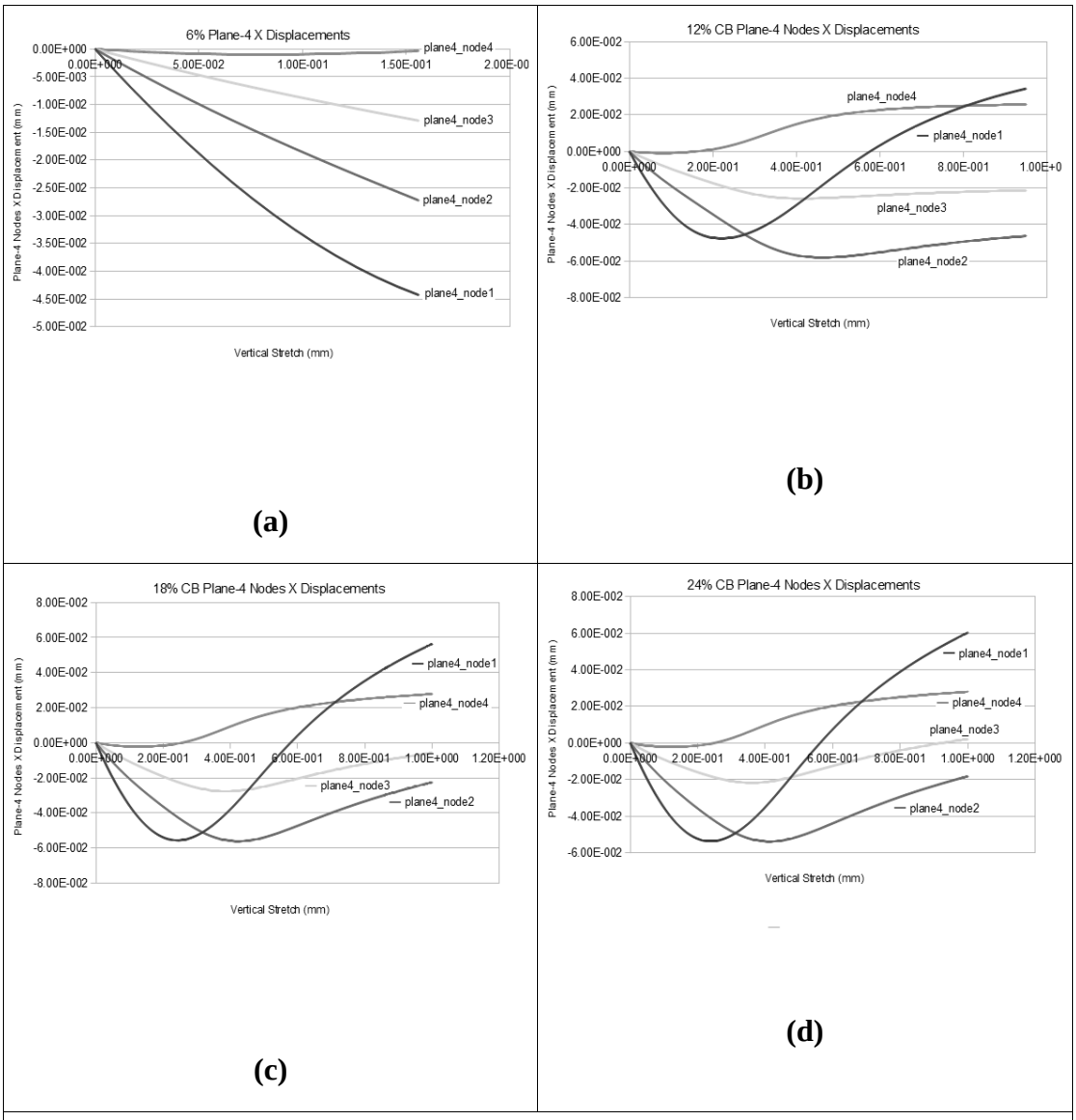

Figure 4.9: X direction displacements for the near-central Plane-4 for all carbon black loadings.

Figure 4.10 shows the comparison of the X displacements of the most displaced node in the auxetic structure, which is the outermost node on the central plane. This region being least restrained by the boundary conditions would naturally experience more freedom in displacement, however the point of interest is the fact that the larger carbon black load cases seem to have displaced more as compared to the lower carbon black load cases.

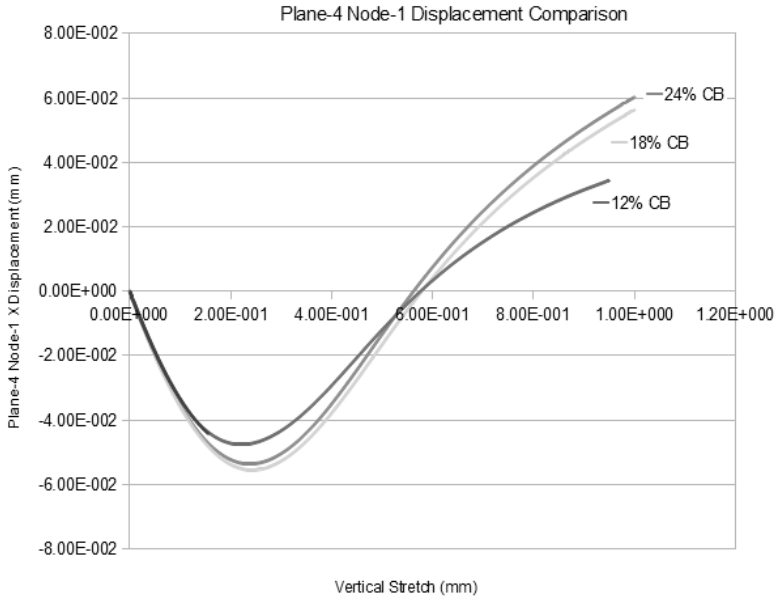

Figure 4.10: Comparison of the X displacement of the most displaced internal node in all the carbon black load cases.

The X displacement comparison for all carbon black load cases in Figure 4.10 shows that the higher carbon black loadings cause a relatively larger displacement in the negative X direction. This can be attributed to the increased stiffness of the ribs and walls. Less stiff walls and rubs in a cellular structure with lower carbon black loading would result in slightly less negative Poisson's ratio effect.

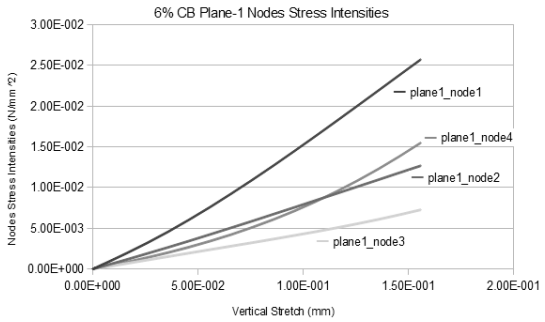

(a) 6% CB Plane-1

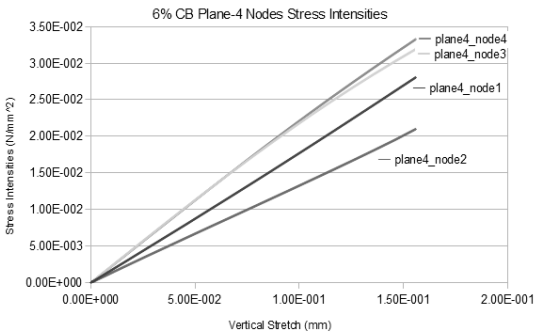

(b) 6% CB Plane-4

Figure 4.11: Plot (a) and (b) show that on the first plane (the one near the pulling surface) has the outermost node experiencing the maximum stress increase with increase in stretch, whereas the maximum stress is experienced by the inner most node for the central plane in the auxetic structure. This trend was observed for the other carbon black load cases as well.

Stress distribution analysis for the vertical stretch showed that the outermost and central portion of the structure experienced the maximum stresses during the extension, as compared to the stresses in the rest of the auxetic structures nodes. This is illustrated by Figure 4.11, which shows the stress distribution for the 6% CB load case for the first plane and the central plane.

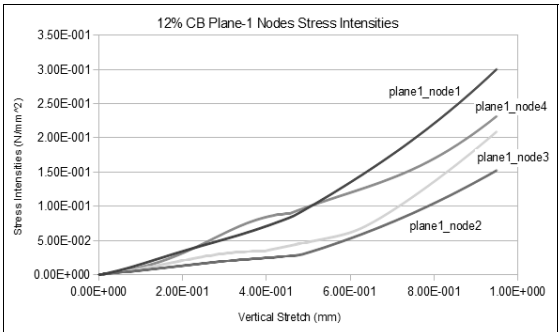

(a) 12% CB Plane-1

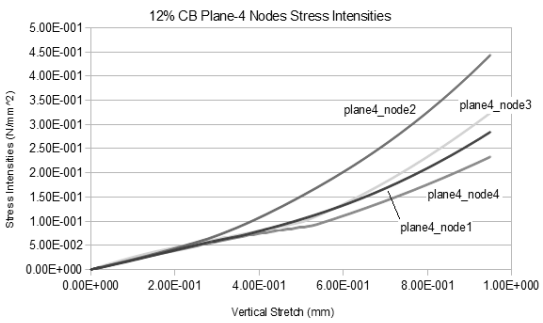

(b) 12% CB Plane-4

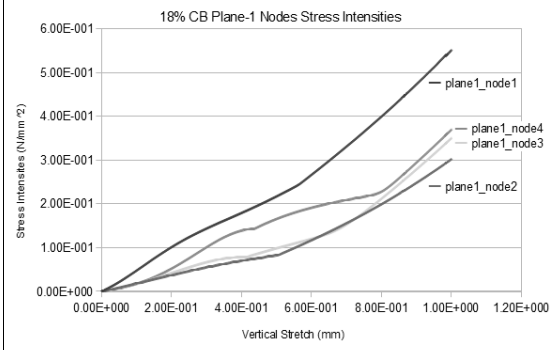

(c) 18% CB Plane-1

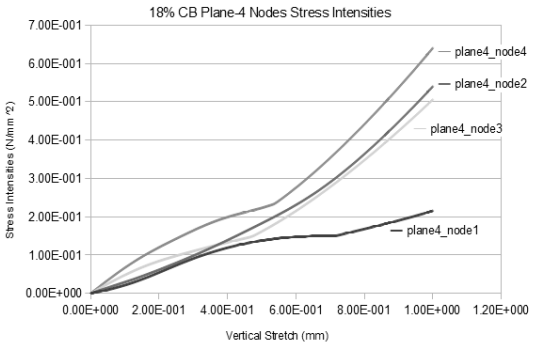

(d) 18% CB Plane-4

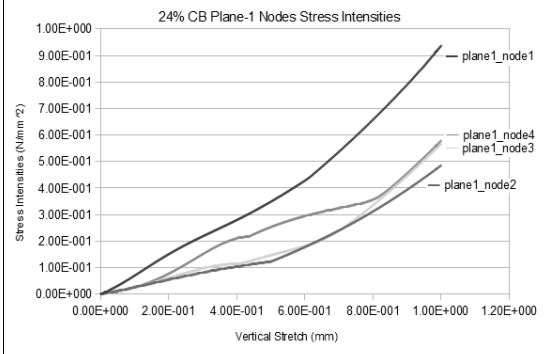

(e) 24% CB Plane-1

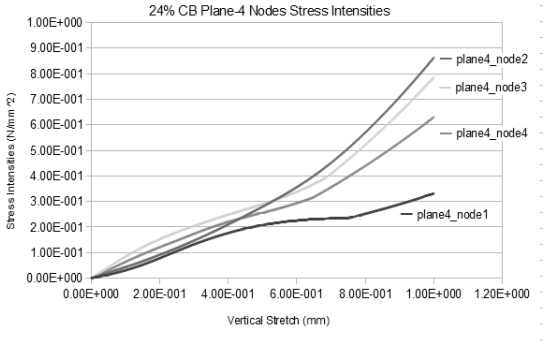

(f) 24% CB Plane-4

Figure 4.12: As shown in Figure 4.11, the other carbon black load cases show higher stresses in the outermost region of the first plane, and the inner most region of the central plane. Also notable is the fact that other than nodes experiencing relatively higher stress, the low stress nodes have a slight fluctuation in stress at a certain point in the stretch.

The rigid nodes rotation also causes a slight depression in the stress-intensity curves shown in Figure 4.12 midway through the stretch. The fluctuation appears to be prominent for some cases whereas for others it is a fairly smooth transition. The increase in stress for the nodes experiencing maximum stress also do not have a linear transition, and the stress increase is higher midway through the stretch. Generally, once the negative Poisson ratio behavior of the auxetic structure has been surpassed by excess extension, the nodes will cease to rotate further, and eventually the overall stress experienced by the structure at various points would increase, as is observed from the sudden increase in stress in the plots for all carbon black load cases.

Also observed in the vertical stretch simulation were the reaction forces at the top surface of the auxetic structure (identified by region (a) in Figure 4.8), which was basically applied a vertical displacement constraint. Figure 4.13 shows a comparative column plot of the maximum stresses experienced by various points over the entire surface of the structure, for all the carbon black load cases for various stretches.

4.6.2 Static horizontal stretch tests

The second set of simulations that were performed for the four cases was of the horizontal stretch. Since the compression to auxeticate was done by compressive forces from the top and from the sides, it was expected that the auxetic behavior would be demonstrated in the perpendicular pull direction as well. However for this case the top surface was not porous and resulted in stress concentration at the top surface, thus resulting in a decreased negative Poisson's ratio behavior from this pull direction. Without cellular porosity at the top and bottom surfaces, the amount of force required to stretch in the direction parallel to these surfaces would increase.

Figure 4.14 shows the vertical displacement for the node on the top surface experiencing the most negative displacement, for the 12%, 18%, and 24% carbon black load cases. Similar auxetic behavior is displayed in this direction as well, however the negative displacement is considerably less as compared to that for the vertical stretch case, a behavior caused by the restraining effect of the non-porous top and bottom surfaces of the foam sheets.

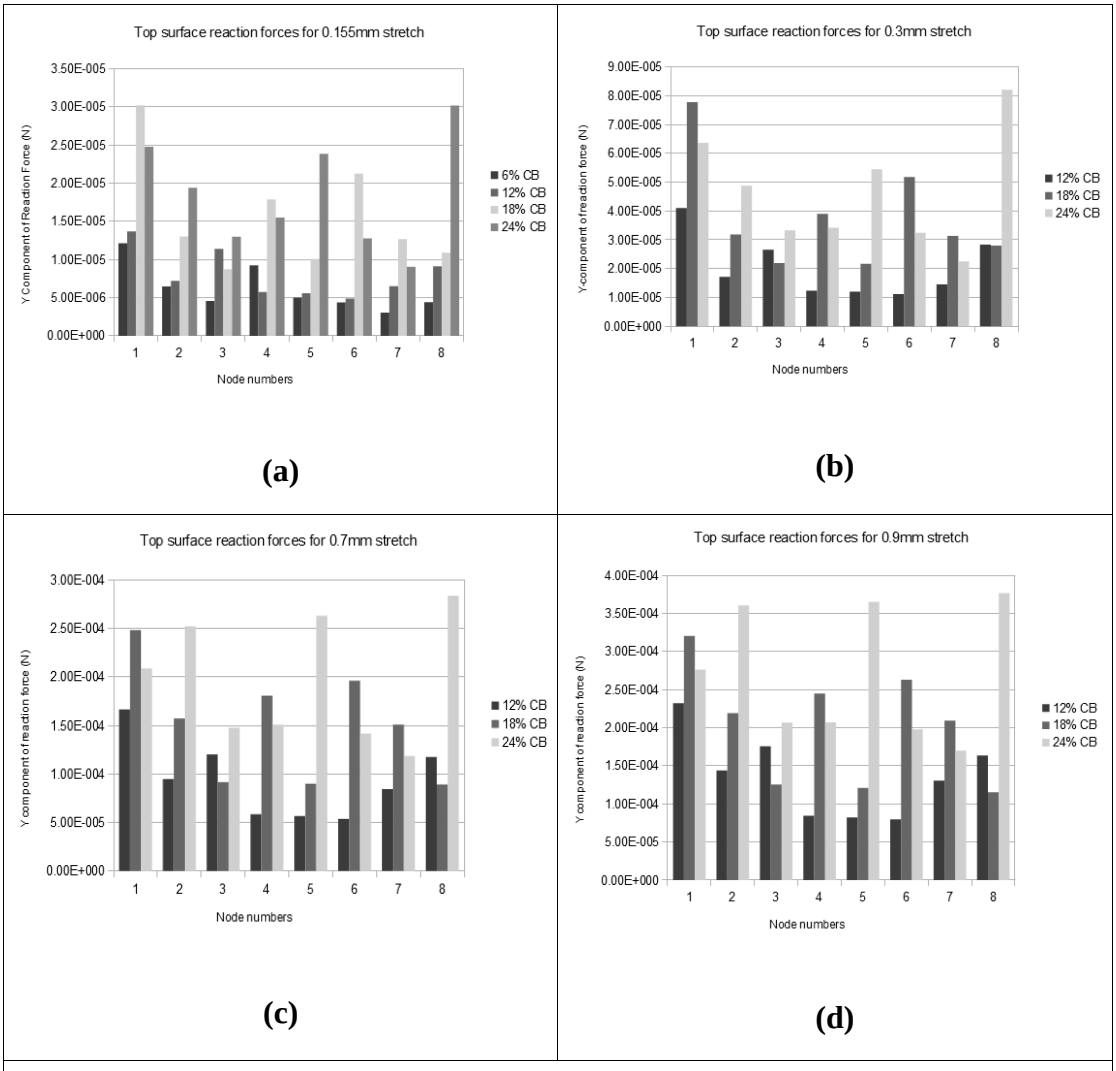

Figure 4.13: Comparison of the Y component of the reaction force at the top pulling surface for all the carbon black load cases. Noticeable is the fact that the reaction force becomes more even at a larger stretch, as can be seen for the 24% carbon black load case. Since the 6% CB case simulation did not exceed more than 0.155mm deformation, the data for it is not represented in the other extension graphs.

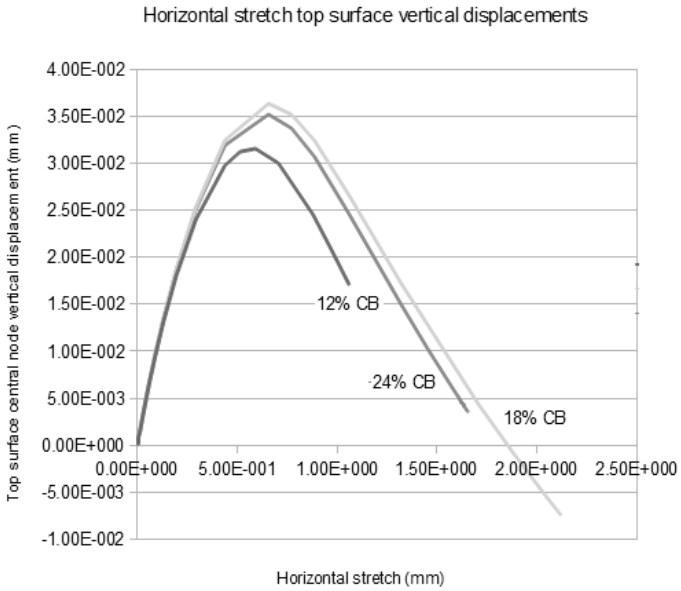

Figure 4.14: Top surface vertical displacements for three carbon black load cases. Note the closeness of the 18% and 24% carbon black loadings, as was observed for the case of the vertical stretch. However the lower carbon black loading 12% has a lesser vertical displacement.

Table 4.2 shows a comparison of the maximum negative displacements for the 12%, 18%, and 24% carbon black load cases.

Table 4.2: Comparison of the negative displacement effect between a vertical and horizontal stretch for the three carbon black loading cases; 12%, 18%, and 24%.

	12% CB	18% CB	24% CB
Vertical Stretch Max. Negative Displacements (mm)	4.76E-002	5.55E-002	5.37E-002
Horizontal Stretch Max. Negative Displacements (mm)	3.24E-002	3.16E-002	3.54E-002

A similar test was performed on the basic spherical void cellular structure model (non-auxetic), and the stress intensities behavior on the top surface for various stretches was observed to be different than that for the auxetic structure. The stress remains fairly evenly distributed throughout the horizontal extension for the nodes, as shown in Figure 4.15. Figure 4.15 also shows the stress contours for about 1mm horizontal stretch for both the non-auxetic and auxetic structures.

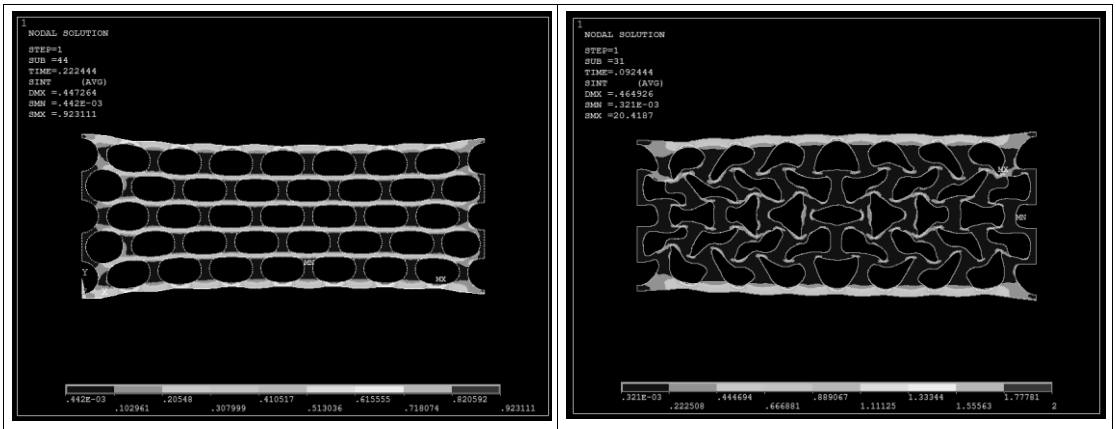

(a) **(b)**

Figure 4.15: Spherical (a) and auxetic (b) adjusted stress contours for around 1mm horizontal stretch. Notice the increased stress concentration for the auextic structure at top surface due to internal nodes rotation and outward push.

The Poisson's ratio in either direction (for the vertical and horizontal stretch tests) is never permanent, and depending on the size of the voids, the rib/wall lengths, increases or decreases, resulting in a more auxetic or less auxetic structure, respectively.

4.6.3 Static full compression tests

The behavior of the idealized auxetic structure was also investigated under a "full-compression" scenario, where sufficient compressive displacement was applied on the top surface to allow the internal auxetic nodes to deform and come into

physical contact with each other. A lightly auxeticated structure was used for this test, since a fully auxeticated structure is already fully compressed, and no further nodal rotations would be possible in that case. The models were compressed statically for a small displacement range, and their nodal X direction displacements, nodal stresses, and top surface Y component of the reaction force was monitored.

It was observed from the nodal displacements in the X direction that the top region of the internal structure did not exhibit negative displacement behavior, and they moved outwards during compression, as is expected from a normal material being compressed. However, it was observed that the central line of nodes in the structure was the most negatively displaced, and that portion moved inwards during the static compression analysis. The region most displaced negatively by the compression was the outer most region in the central plane, as shown in image (a) of Figure 4.16. This region was observed to be the most displaced inwards during the compression for all carbon black load cases. However the central portion of the structure did not show any remarkable auxetic behavior since it experienced compression from all directions.

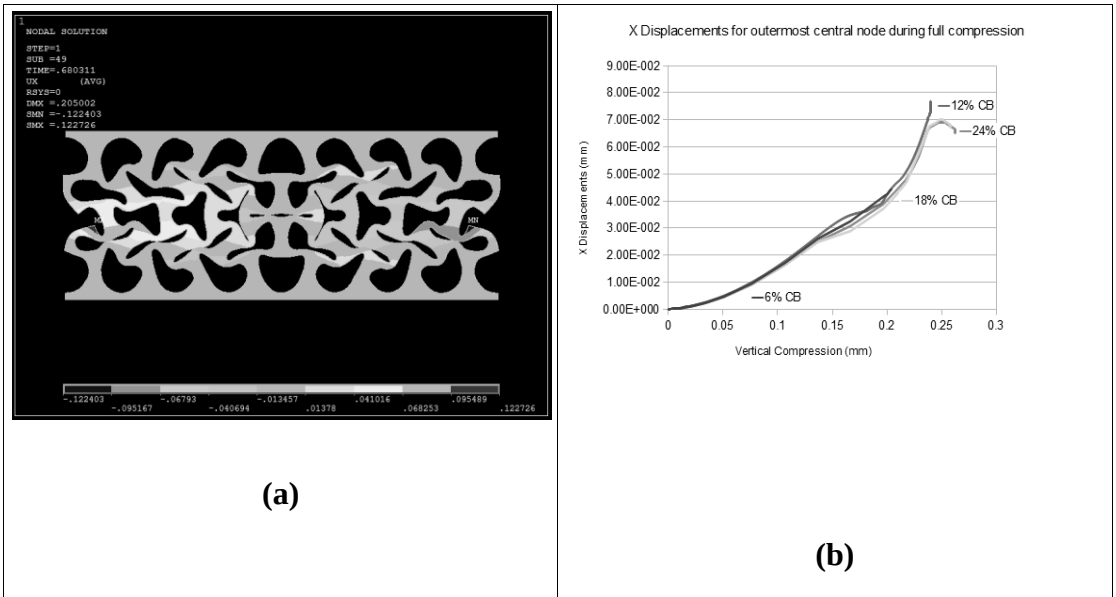

(a)

(b)

Figure 4.16: The typical compressive behavior exhibited by all four carbon black loadings is shown in (a). The contour shows most inward displacement during compression by the outermost region of the central plane. Image (b) shows the displacement behavior for this region for all carbon black loadings, with no significant difference between them apart from fluctuations due to alignment of the nodes in the structure due to compression and resulting contact.

Contact is most apparent in the central region due to the ease of adjustment of the re-entrant auxetic structure, with the outer regions more bound to the rigid boundaries, this experiencing minimal deformation and nodal rotation. The reaction force at the top surface has an abrupt change when contact is established in the inner region, thus a greater force is required to further compress the material as the re-entrant structure has fully collapsed. This is shown in Figure 4.17, where the reaction force experienced by the structure increases with increasing carbon black loading.

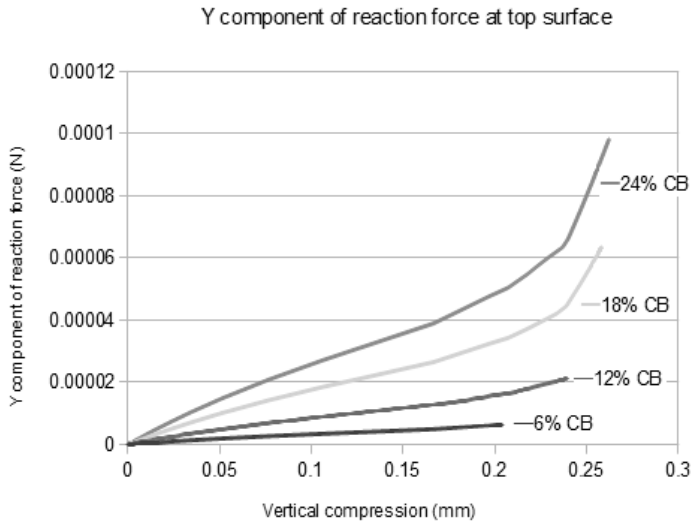

Figure 4.17: Increasing Y component of the reaction force with increasing carbon black loading. Note the abrupt change in the almost linear increase in the reaction force after around 0.2mm of compression.

Complete structural collapse after a certain extent of compression would induce material rigidity, thus impeding further compression. A foam without a re-entrant structure would achieve rigidity at a larger compression. A higher carbon black loading for a given cell size would thus give greater shock absorbing capacity.

4.6.4 Static object penetration tests

The compressive behavior was taken one step further with contact and

penetration of a fairly small object on the surface of the foam. Small objects would naturally induce a greater stress at the point of contact. Depending on the object size, the distribution of the stress generated would vary, and so would the internal nodal rotations and displacements due to the compression on a small portion of the structure.

Figure 4.18 shows the adjusted stress contours for all four carbon black load cases. The stress contours have been adjusted to show 0.3 N/mm^2 as the highest stress in the structures for all cases, which allows better comparative visualization of the stress distribution for all load cases.

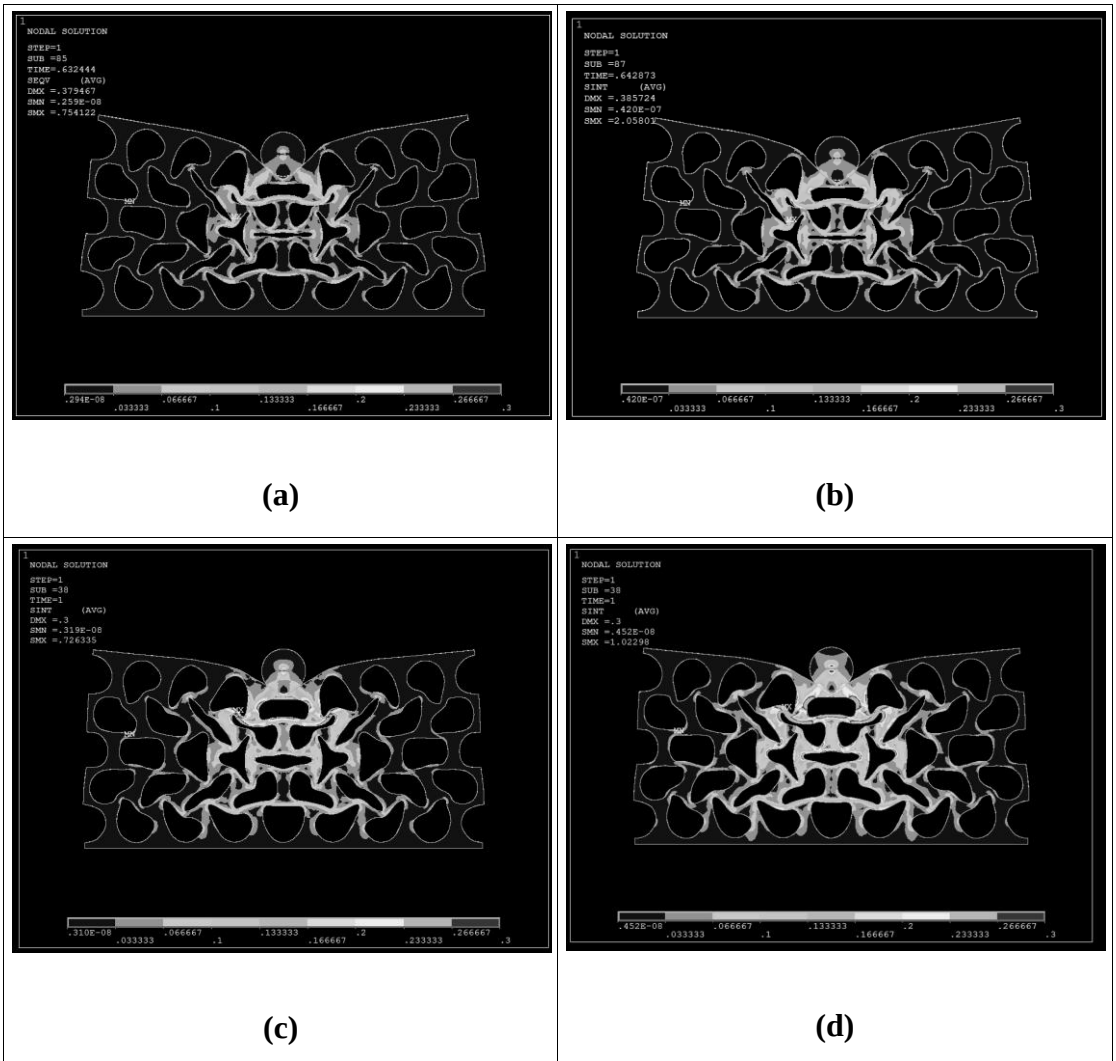

(a) **(b)**

(c) **(d)**

Figure 4.18: Stress distribution contours for all carbon black loadings for the case of a small body contact and penetration. The ball is of 0.2mm radius. Notable is the fact that a higher stress is generated directly below the point of contact, before foam densification has started.

The degree of penetration would be reduced for an auxetic compression case, thus allowing localized rearrangement of the internal re-entrant structure. In severe impact situations, however, very small high velocity objects can cause tearing of the material. A higher carbon black loading would, again, prove useful in small object contact-penetration and moderate impact as well. Where direct contact of a high velocity small projectile is to be avoided, a relatively thinner vulcanized rubber sheet can be used on the top surface which would help avoid unwanted penetration into the cellular structure, and still provide the required shock absorbing capabilities.

4.6.5 Viscoelastic curve-fitting

Experimental data was obtained in the form of force decay curves, which were converted to shear modulus vs. time curves by standard calculations. These shear modulus vs. time curves were fed to the ANSYS Viscoelastic curve fitting tool, where 3 shear parameters were provided for curve fitting. Values were adjusted manually to carefully obtain the closest fit for the experimental curves. The respective curve-fit results are shown in Figure 4.19.

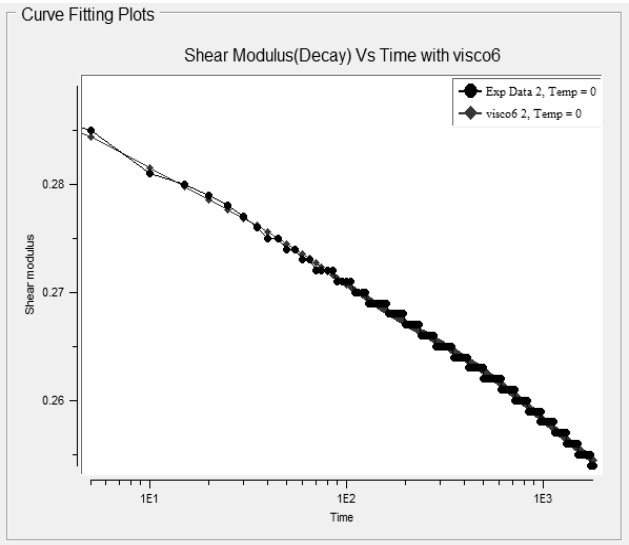

(a) 6% CB

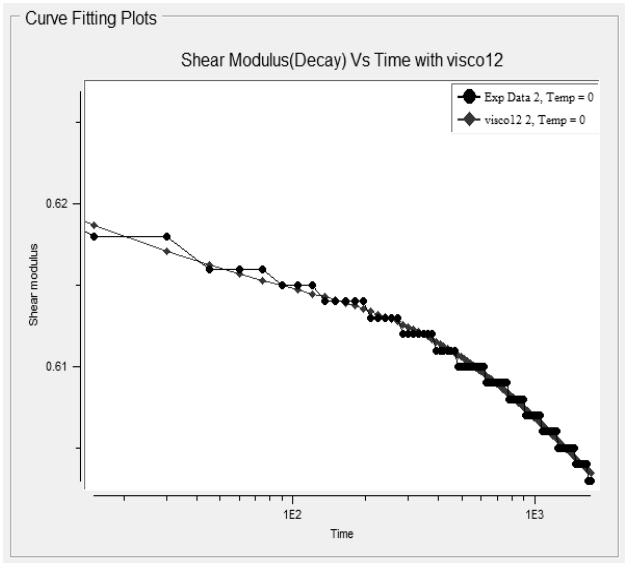
Curve Fitting Plots
Shear Modulus(Decay) Vs Time with visco12
Exp Data 2, Temp = 0
visco12 2, Temp = 0
0.62
0.61
Shear modulus
1E2
1E3
Time

(b) 12% CB

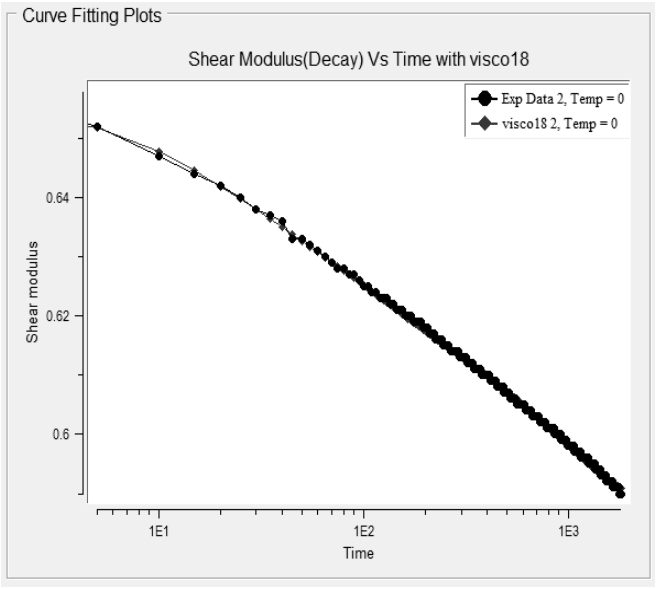
Curve Fitting Plots
Shear Modulus(Decay) Vs Time with visco18
Exp Data 2, Temp = 0
visco18 2, Temp = 0
0.64
0.62
0.6
Shear modulus
1E1
1E2
1E3
Time

(c) 18% CB

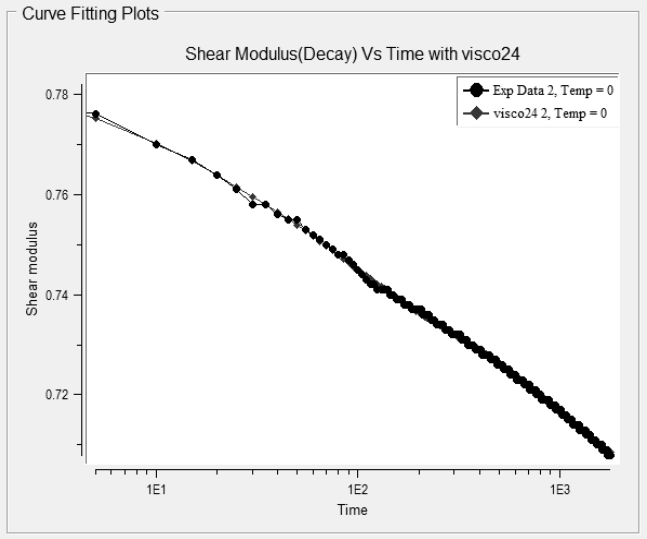

(d) 24% CB

Figure 4.19: Curve fitting data and plots for all carbon black load cases.

4.6.6 Transient stretch analyses using time dependent properties

Tests were performed for the 24% carbon black loaded material which used viscoelastic properties in addition to the hyperelastic properties. In order to achieve this, transient analyses were performed using the same loading conditions used in previous static analyses, the difference here being the retention of the displacement for a certain period of time to observe the effect of stress relaxation properties on the auxetic cellular structure. It was observed, however, that the stress relaxation properties had minimal effect on the overall time-dependent behavior of the material post-loading.

Vertical stretch was performed for 24% carbon black loaded sample. The results were observed in the form of nodal displacements and adjustments with time, when the amount of stretch was kept constant for a duration of 5 seconds. The decay in the top surface reaction force was observed. The decay was linear and of very small magnitude, thus showing that the base material's own viscoelastic properties play little role in determining the overall viscoelastic behavior of a low density cellular structure. The nodal displacements were also observed to be negligible during the 5

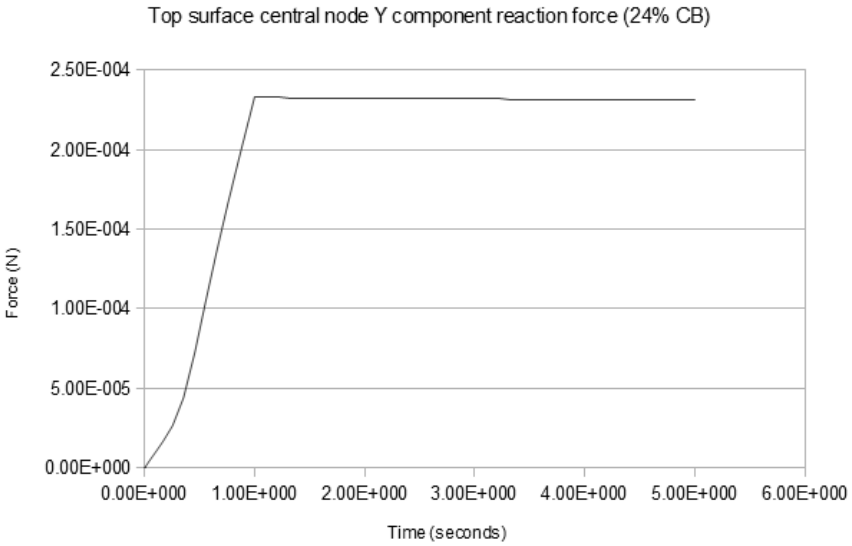

Figure 4.20: Top surface reaction force decay for a 24% carbon black loaded specimen. Notice that the decay is fairly unnoticable and is almost linear.

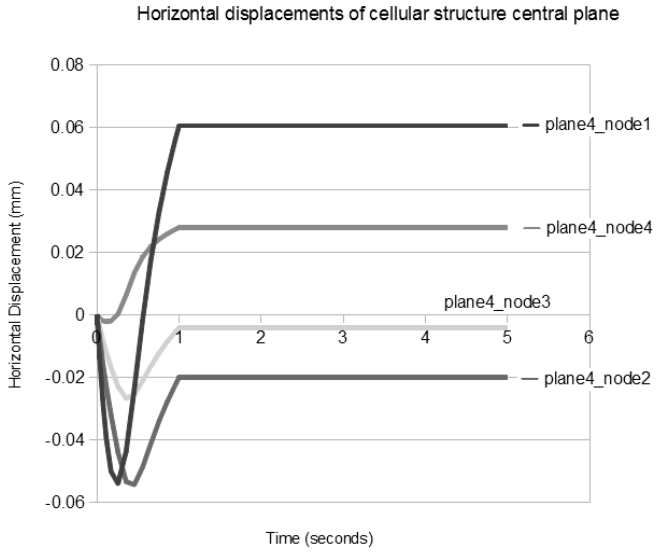

Figure 4.21: Central plane nodal displacements for the 24% carbon black case for the 5 second duration. Initial ramp loading phase shows reversal in nodal displacements with time (and stretch), and is observed to be fairly constant during the displacement hold.

second stretch hold.

Horizontal displacement due to viscoelastic effects for the vertical stretch case were also observed to be small. Figure 4.21 shows the horizontal displacements for

the nodes in the central plane (Plane-4), and it is observed that the nodal displacements experience negative displacement for a certain amount of stretch, and then their displacement direction reverses. However, their displacements are fairly negligible during the displacement hold phase, where the material is expected to exhibit viscoelastic stress relaxation behavior due to the constant stretch applied.

Figure 4.22 shows the outermost node's displacement trend during the displacement holding phase only.

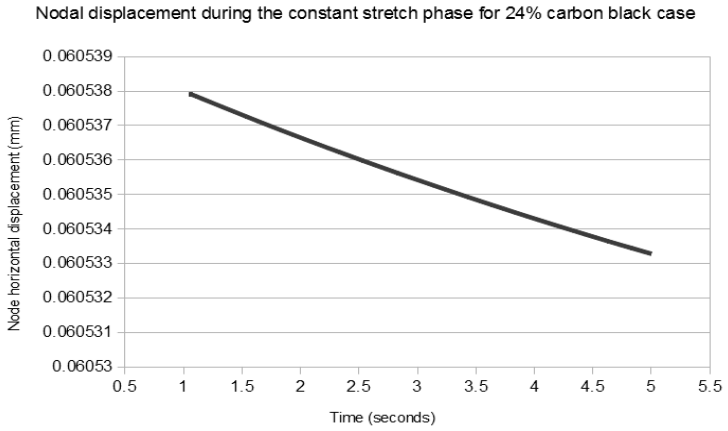

Figure 4.22: Outermost nodal displacement of central plane on the 24% carbon black loaded structure, for the case of the vertical stretch. Note the small variation in displacement with time.

The nodal displacements for all cases during the hold are in the negative direction, showing that the negative Poisson ratio effect will be prevalent even during the post-reversal phase, which implies that a stretch cellular auxetic foam made of rubber would tend to relax in the negative Poisson ratio direction. Since the viscoelastic effects in cellular structures due to the effect of trapped air and its diffusion were not taken into account for this simulation, it is assumed in this research that the slow diffusion of the air in the stretch state would slow down the nodal displacements over time, and the nodal displacements in the negative direction during relaxation would be even less noticeable. A similar test was performed on a solid rubber specimen of almost the same dimensions. However the solid rubber specimen experienced post-stretch contraction at a relatively slower rate as compared to that for the auxetic cellular structure. This is primarily due to the low density for the cellular structure, resulting in more room for structural deformations that are fairly quicker

than slow molecular adjustments due to viscoelastic effects.

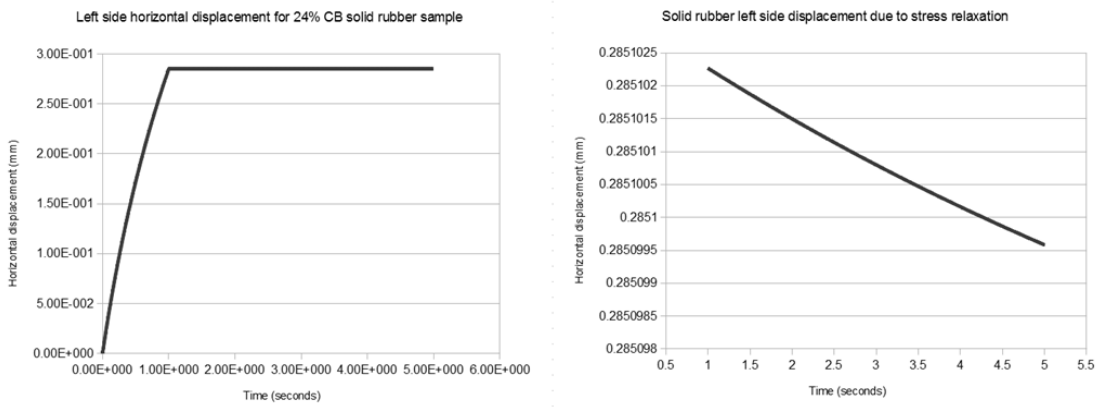

Figure 4.23: Stress relaxation effects on a solid rubber specimen stretched vertically.

Compressed auxetic structures were also analyzed for viscoelastic effects. However, due to collapse of the cellular structure and high densification due to a greater compression results in a nearly non-porous structure, thus leaving no room for any noticeable auxetic effects. It should be observed, however, that since an auxetic structure causes stress distribution over a wide region due to re-entrant cellular structure's adjustments, this distribution would tend to localize in a relatively smaller region due to stress-relaxation effects, if the compression is kept constant for a reasonable amount of time.

CONCLUSIONS

The purpose of this work was to investigate the behavior of an idealized auxetic structure under various loading conditions using base material mechanical properties. A study of the results obtained from the simulations led to the following conclusions about the nature of natural rubber based auxetic cellular structures:

5. Carbon black loadings for a given auxetic cellular structure resulted in slightly different negative Poisson ratio behavior, although stress distributions and reaction forces varied considerably. Manufacturing process may, however, result in foams of varying density for different carbon black loadings, hence Poisson ratio is expected to vary.
6. The tests were performed for a small portion of a 2mm thick vulcanized natural rubber auxetic foam, and hence the top and bottom surfaces were modeled as non-porous, while the sides were porous. The difference in the negative Poisson's ratio effect in loading directions perpendicular to each other was observed to be considerable, thus ascertaining the fact that for an idealized auxetic structure for a vulcanized rubber specimen, the Poisson's ratio would be dependent on the loading direction.
7. The negative Poisson's ratio behavior would not be observable for the entire stretch applied to the auxetic foam, but would be limited to a certain stretch, depending on the density of the foam, and the size of the voids. This effect would be fairly similar for carbon black loadings studied in this work due to the fact that structure deformations would be more responsible for the negative Poisson's ratio effect rather than the carbon black loading itself. A mild difference in the Poisson's ratio for different carbon black loadings would be observable due to the fact that higher loadings would render the base material more rigid.
8. Small and large body contact and penetration analyses showed the re-entrant structure deforming with increasing compression, with the area of the internal re-entrant structure disturbed changing with the size of the body coming in contact with the auxetic cellular structure. A small object with dimensions

slightly larger than the dimensions of the voids in the cellular structure would result in limited auxetic structure adjustments. However, the full compression tests performed showed the wave of internal structural re-organization spanning the entire length of the region of contact with the external body.

9. Applications where moderate impact loads and prolonged compression is required may benefit from natural rubber based auxetic cellular structures. Natural rubber based cellular auxetic materials can be used as part of a multi-layered composite structure to impart superior properties for demanding applications. For example, the natural rubber auxetic foam sheet can be used with a solid rubber sheet to increase impact sustaining properties for various sports and self-defense applications. The reduced weight due to the cellular structure and the unique properties of the re-entrant structure would result in better stress distribution.

FUTURE WORK

Based on the results obtained from the experimental and simulation work, several future work items are suggested which would help in providing a better understanding for the feasibility and applicability of this fairly untouched class of auxetic cellular foams.

1. The development of natural rubber based auxetic cellular structures by a single step process needs to be worked on. This would most probably require the development of a special die which would allow thickness adjustment of the die cavity during the vulcanization curing phase.
2. The investigation needs to be extended to even higher carbon black loadings to observe the effect of considerably different properties of base material on the auxetic behavior, and the negative Poisson's ratio effect.
3. Three dimensional models need to be developed to investigate the deformation characteristics of idealized or X-Ray tomographically scanned auxetic cellular structures developed from the aforementioned one-step manufacturing process. This would give a more accurate represenation and analysis of the auxetic structure.
4. Foam viscoelastic effects due to air present inside the voids needs to be inevestigated in future research for natural rubber based auxetic cellular structures.
5. More viscoelastic properties for the base material including the glass transition temperature would help in running simulations for high velocity impact scenarios, where the material is expected to stiffen when the rate of loading is extremely high. Dynamic Mechanical Thermal Analyses for the base natural rubber would have to be investigated to determine different viscoelastic properties.
6. Combination of natural rubber based auxetic cellular structures with non-elastomeric materials used for various structural applications needs to be investigated to observe the effect of the auxetic cellular structure on different mechanical loading scenarios.

References

[1] L. J. Gibson and M. F. Ashby, *Cellular Solids: Structure and Properties*, 2nd ed. Cambridge University Press, 1999.

[2] A. Bezazi and F. Scarpa, "Mechanical behaviour of conventional and negative Poisson's ratio thermoplastic polyurethane foams under compressive cyclic loading," *International Journal of Fatigue*, vol. 29, no. 5, pp. 922 – 930, 2007.

[3] N. Chan and K. Evans, "Fabrication methods for auxetic foams," *Journal of Materials Science*, vol. 32, no. 22, pp. 5945–5953, 1997.

[4] N. Chan and K. Evans, "Microscopic examination of the microstructure and deformation of conventional and auxetic foams," *Journal of Materials Science*, vol. 32, no. 21, pp. 5725–5736, 1997.

[5] M. Bianchi, F. Scarpa, and C. Smith, "Stiffness and energy dissipation in polyurethane auxetic foams," *Journal of Materials Science*, vol. 43, no. 17, pp. 5851–5860, 2008.

[6] A. Alderson, K. Alderson, P. Davies, and G. Smart, "A process for the production of auxetic foams," U.S. Patent EP2042252B129-Jun-2011.

[7] E. A. Friis, R. S. Lakes, and J. B. Park, "Negative Poisson's ratio polymeric and metallic foams," *Journal of Materials Science*, vol. 23, no. 12, pp. 4406–4414, 1988.

[8] W. Miller, Z. Ren, C. W. Smith, and K. E. Evans, "A negative Poisson's ratio carbon fibre composite using a negative Poisson's ratio yarn reinforcement," *Composites Science and Technology*, vol. 72, no. 7, pp. 761 – 766, 2012.

[9] M. Ramírez, G. G. Nava-Gómez, F. J. Sabina, H. Camacho-Montes, R. Guinovart-Díaz, R. Rodríguez-Ramos, and J. Bravo-Castillero, "Enhancement of Young's moduli and auxetic windows in laminates with isotropic constituents," *International Journal of Engineering Science*, vol. 58, no. 0, pp. 95 – 114, 2012.

[10] M. Assidi and J.-F. Ganghoffer, "Composites with auxetic inclusions showing both an auxetic behavior and enhancement of their mechanical properties," *Composite Structures*, vol. 94, no. 8, pp. 2373 – 2382, 2012.

[11] T. Xu and G. Li, "A shape memory polymer based syntactic foam with negative Poisson's ratio," *Materials Science and Engineering: A*, vol. 528, no. 22–23, pp. 6804 – 6811, 2011.

[12] J. P. M. Whitty, B. Henderson, J. Francis, and N. Lloyd, "Optimized thick-wall cylinders by virtue of Poisson's ratio selection: Part 1: Isochoric pressure application," *Nuclear Engineering and Design*, vol. 241, no. 8, pp. 2766 – 2774, 2011.

[13] F. D. Reis and J. F. Ganghoffer, “Equivalent mechanical properties of auxetic lattices from discrete homogenization,” *Computational Materials Science*, vol. 51, no. 1, pp. 314 – 321, 2012.

[14] Y. Prawoto, “Seeing auxetic materials from the mechanics point of view: A structural review on the negative Poisson’s ratio,” *Computational Materials Science*, vol. 58, no. 0, pp. 140 – 153, 2012.

[15] A. Spadoni and M. Ruzzene, “Elasto-static micropolar behavior of a chiral auxetic lattice,” *Journal of the Mechanics and Physics of Solids*, vol. 60, no. 1, pp. 156 – 171, 2012.

[16] J. Dirrenberger, S. Forest, and D. Jeulin, “Elastoplasticity of auxetic materials,” *Computational Materials Science*, vol. 64, no. 0, pp. 57 – 61, 2012.

[17] N. Mills, *Polymer Foams Handbook - Engineering and Biomechanics Applications and Design Guide*, 1st ed. Butterworth-Heinemann, 2007.

[18] E.-K. Lee and S.-Y. Choi, “Preparation and characterization of natural rubber foams: Effects of foaming temperature and carbon black content,” *Korean Journal of Chemical Engineering*, vol. 24, no. 6, pp. 1070–1075, 2007.

[19] L. M. Yang and V. P. W. Shim, “A visco-hyperelastic constitutive description of elastomeric foam,” *International Journal of Impact Engineering*, vol. 30, no. 8–9, pp. 1099 – 1110, 2004.

[20] S. Alvermann, “Effective viscoelastic behavior of cellular auxetic materials,” Graz University of Technology, Institute of Applied Mechanics.

[21] J. G. F. Wismans, J. A. W. van Dommelen, L. E. Govaert, and H. E. H. Meijer, “X-ray computed tomography based modelling of polymer foams,” *Materials Science Forum*, vol. 638–6, pp. 2761–2765, 2010.

[22] S. A. McDonald, N. Ravirala, P. J. Withers, and A. Alderson, “In situ three-dimensional X-ray microtomography of an auxetic foam under tension,” *Scripta Materialia*, vol. 60, no. 4, pp. 232 – 235, 2009.

[23] F. Zhu, C. C. Chou, and K. H. Yang, “Shock enhancement effect of lightweight composite structures and materials,” *Composites Part B: Engineering*, vol. 42, no. 5, pp. 1202 – 1211, 2011.

[24] X. Yang, Y. Xia, and Q. Zhou, “Influence of stress softening on energy-absorption capability of polymeric foams,” *Materials & Design*, vol. 32, no. 3, pp. 1167 – 1176, 2011.

[25] K. C. Guriya and D. K. Tripathy, “Morphology and physical properties of closed-cell microcellular ethylene–propylene–diene terpolymer (EPDM) rubber vulcanizates: Effect of blowing agent and carbon black loading,” *Journal of Applied Polymer Science*, vol. 62, no. 1, pp. 117–127, 1996.

[26] D. Weaire and R. Phelan, “A counter-example to Kelvin’s conjecture on minimal surfaces,” *Philosophical Magazine Letters*, vol. 69, no. 2, pp. 107–

110, 1994.

[27] M. Bouakba, A. Bezazi, and F. Scarpa, “FE analysis of the in-plane mechanical properties of a novel Voronoi-type lattice with positive and negative Poisson’s ratio configurations,” *International Journal of Solids and Structures*, vol. 49, no. 18, pp. 2450 – 2459, 2012.

[28] M. D. Montminy, A. R. Tannenbaum, and C. W. Macosko, “The 3D structure of real polymer foams,” *Journal of Colloid and Interface Science*, vol. 280, no. 1, pp. 202 – 211, 2004.

[29] J. N. Grima, R. Gatt, N. Ravirala, A. Alderson, and K. E. Evans, “Negative Poisson’s ratios in cellular foam materials,” *Materials Science and Engineering: A*, vol. 423, no. 1–2, pp. 214 – 218, 2006.

[30] M. Bianchi, F. Scarpa, M. Banse, and C. W. Smith, “Novel generation of auxetic open cell foams for curved and arbitrary shapes,” *Acta Materialia*, vol. 59, no. 2, pp. 686 – 691, 2011.

[31] J. Ju, D.-M. Kim, and K. Kim, “Flexible cellular solid spokes of a non-pneumatic tire,” *Composite Structures*, vol. 94, no. 8, pp. 2285 – 2295, 2012.

[32] L. J. Lee, C. Zeng, X. Cao, X. Han, J. Shen, and G. Xu, “Polymer nanocomposite foams,” *Composites Science and Technology*, vol. 65, no. 15–16, pp. 2344 – 2363, 2005.

[33] J. E. Mark, B. Erman, and F. R. Eirich, *Science and technology of rubber*. .

[34] G. Zhao, L. Shi, D. Zhang, X. Feng, S. Yuan, and J. Zhuo, “Synergistic effect of nanobarite and carbon black fillers in natural rubber matrix,” *Materials &; Design*, p. -, 2011.

[35] S. Ngamsurat, K. Boonkerd, U. Leela-adisorn, and P. Potiyaraj, “Curing Characteristics of Natural Rubber Filled with Gypsum,” *Energy Procedia*, vol. 9, pp. 452 – 458, 2011.

[36] J.-B. Donnet, *Carbon Black: Science and Technology*. CRC Press, 1993.

[37] J. S. Dick, C. Harmon, and A. Vare, “Quality assurance of natural rubber using the rubber process analyzer,” *Polymer Testing*, vol. 18, no. 5, pp. 327 – 362, 1999.

[38] H. Brown, *Rubber - Its sources, cultivation, and preparation*. John Murray, Albemarle Street, W. London, 1914.

[39] N. Rattanasom, S. Prasertsri, and T. Ruangritnumchai, “Comparison of the mechanical properties at similar hardness level of natural rubber filled with various reinforcing-fillers,” *Polymer Testing*, vol. 28, no. 1, pp. 8 – 12, 2009.

[40] J. B. van Beilen and Y. Poirier, “Establishment of new crops for the production of natural rubber,” *Trends in Biotechnology*, vol. 25, no. 11, pp. 522 – 529, 2007.

[41] K. Nawamawat, J. T. Sakdapipanich, C. C. Ho, Y. Ma, J. Song, and J. G.

Vancso, “Surface nanostructure of Hevea brasiliensis natural rubber latex particles,” *Colloids and Surfaces A: Physicochemical and Engineering Aspects*, vol. 390, no. 1–3, pp. 157 – 166, 2011.

[42] C. Nah, J. Jose, J.-H. Ahn, Y.-S. Lee, and A. N. Gent, “Adhesion of carbon black to elastomers,” *Polymer Testing*, vol. 31, no. 2, pp. 248 – 253, 2012.

[43] MSC Software, “Nonlinear finite element analysis of elastomers.” [Online]. Available: http://www.axelproducts.com/downloads/MARC_FEA_ELASTOMERS_2000.pdf. [Accessed: 30-Sep-2011].

[44] S. Kaang and C. Nah, “Fatigue crack growth of double-networked natural rubber,” *Polymer*, vol. 39, no. 11, pp. 2209 – 2214, 1998.

[45] A. Bhattacharya, J. W. Rawlins, P. Ray - *Polymer grafting and crosslinking.* Wiley; 1st edition (December 22, 2008).

[46] R. F. Grossman, *The mixing of rubber*. Springer, 1st edition (January 15, 2007).

[47] D. Eaves, *Handbook of Polymer Foams*. Rapra Technology Limited, 2004.

[48] J. H. Kim, K. C. Choi, J. M. Yoon, “The foaming characteristics and physical properties of natural rubber foams - Effects of carbon black content and foaming pressure.”

[49] B. S. Zhang, X. F. Lv, Z. X. Zhang, Y. Liu, J. K. Kim, and Z. X. Xin, “Effect of carbon black content on microcellular structure and physical properties of chlorinated polyethylene rubber foams,” *Materials & Design*, vol. 31, no. 6, pp. 3106 – 3110, 2010.

[50] Z. M. Ariff, Z. Zakaria, L. H. Tay, and S. Y. Lee, “Effect of foaming temperature and rubber grades on properties of natural rubber foams,” *Journal of Applied Polymer Science*, vol. 107, no. 4, pp. 2531–2538, 2008.

[51] N. N. Najib, Z. M. Ariff, A. A. Bakar, and C. S. Sipaut, “Correlation between the acoustic and dynamic mechanical properties of natural rubber foam: Effect of foaming temperature,” *Materials & Design*, vol. 32, no. 2, pp. 505 – 511, 2011.

[52] J. Bonnet and R. Wood, *Nonlinear continuum mechanics for finite element analysis*. Press syndicate of The University of Cambridge, 1997.

[53] M. J. G. Ruiz and L. Y. S Gonzalez, “Comparison of hyperelastic material models in the analysis of fabrics,” *International Journal of Clothing Science and Technology*, vol. 18, no. 5, pp. 314–325, 2006.

[54] M. Meyers and K. Chawla, *Mechanical Behavior of Materials*. Cambridge University Press, 2009.

[55] Sheldon Imaoka, TSE ANSYS, “Analyzing viscoelastic materials.” *ANSYS Advantage*, Volume 2, Issue 4, 2008.

[56] A. Alderson, K. Alderson, P. Davies, and G. Smart, “A process for the preparation of auxetic foams,” U.S. Patent EP 2 042 252 B101-Apr-2009.

[57] L. Laiarinandrasana, A. Jean, D. Jeulin, and S. Forest, “Modelling the effects of various contents of fillers on the relaxation rate of elastomers,” *Materials & Design*, vol. 33, pp. 75 – 82, 2012.